Internal structure, ice content and dynamics of Ölgrube and Kaiserberg rock glaciers (Ötztal Alps, Austria) determined from geophysical surveys.

Helmut HAUSMANN[1)4)*)], Karl KRAINER[2)], Ewald BRÜCKL[1)] & Christian ULLRICH[3)]

[1)] Institute of Geodesy and Geophysics, Vienna University of Technology, Vienna, Austria;

[2)] Institute of Geology and Paleontology, University of Innsbruck, Innsbruck, Austria;

[3)] Federal Office of Metrology and Surveying (BEV), Vienna, Austria;

[4)] Central Institute for Meteorology and Geodynamics (ZAMG), Vienna, Austria;

[*)] Corresponding author, helmut.hausmann@zamg.ac.at

KEYWORDS

mountain permafrost
Eastern Alps
rock glacier
geophysics
creep

Abstract

In this study we use a concept based on three geophysical methods (Ground-penetrating radar / GPR, seismic refraction, gravimetry) to provide new insight into the internal structure, ice content and dynamics of the two active rock glaciers Ölgrube and Kaiserberg. Both rock glaciers are located in side valleys of the Kauner Valley (Ötztal Alps, Austria) and consist of debris derived from orthogneiss, paragneiss and mica schist. At both rock glaciers we determined a 4 - 6 m thick debris layer at the surface (active layer), underlain by 20 - 30 m of ice-rich permafrost, and 10 - 15 m of ice-free sediments. The average depth to the bedrock was found in 35 - 50 m. Estimated volumetric ice contents vary between 40 and 60 % based on our field measurements. Structural and physical parameters derived from the mentioned surface based geophysical methods are used to explain the dynamics of the rock glaciers. From the two rock glaciers that were investigated in this study and one additional rock glacier, which was investigated by applying the same methodology in an earlier study, we found a parameter that describes their creep behaviour and shows that the three geophysical models are conclusive. Concerning the dynamics of these active rock glaciers, the data indicate that a reduction of the ice content causes an increase of internal friction, lower seismic P-wave velocities, and higher bulk densities. In order to keep a degrading rock glacier in motion a thickening is required. The GPR-reflection patterns of the permafrost layer and their relation to the structural and physical parameters primarily reveal that long reflectors parallel to the surface are found in regions with high P-wave velocity and low density, indicating zones with high ice content.

In dieser Arbeit wird eine Kombination aus drei geophysikalischen Methoden (Georadar, Refraktionsseismik, Gravimetrie) angewandt, um Erkenntnisse über die interne Struktur, den Eisgehalt und die Dynamik der beiden aktiven Blockgletscher Ölgrube und Kaiserberg zu gewinnen. Die beiden Blockgletscher befinden sich in Seitentälern des Kaunertals (Ötztaler Alpen, Tirol) und bestehen aus Schuttmaterial, das durch die Verwitterung von Orthogneis, Paragneis und Glimmerschiefer im Einzugsgebiet entstanden ist. Aus den geophysikalischen Modellen resultieren für beide Blockgletscher ein vierschichtiger Aufbau: eine 4 - 6 m dicke ungefrorene Schuttlage („active layer“), darunter 20 - 30 m eisreicher Permafrost und 10 - 15 m eisfreie Sedimente. Das Festgestein schließlich wurde in 35 - 50 m Tiefe detektiert. Der Wert für den Eisgehalt variiert zwischen 40 und 60 vol%. Die Kenntnis der resultierenden Strukturen und physikalischen Parameter dient dazu, das dynamische Verhalten von Blockgletschern zu erklären. Durch den Vergleich der beiden Blockgletscher und eines dritten, der mit denselben Methoden in einer früheren Studie bearbeitet wurde, konnte eine gemeinsame Schätzgröße gefunden werden, die das Kriechverhalten beschreibt und die Ergebnisse der geophysikalischen Modelle unterstützt. Es konnte herausgefunden werden, dass eine Reduktion des Eisgehalts zu einer Erhöhung der internen Reibung, einer geringeren seismischen P-Wellengeschwindigkeit und einer höheren Dichte führt. Die Reflexionsmuster aus dem Permafrost zeigen, dass lange, oberflächen-parallele Reflektoren in Gebieten mit höherer seismischer P-Wellengeschwindigkeit und geringer Dichte vorkommen und daher eisreiche Zonen repräsentieren.

1. Introduction

The internal structure and the ice content of active rock glaciers are important for investigating the geotechnical behaviour of alpine permafrost, for understanding the genesis of these landforms and for predicting their future response to climate change. Other questions are based on structural and physical parameters and relate to the sediment storage where rock glaciers are important parameters for sediment budget analyses (Barsch and Jakob, 1998; Otto et al., 2009). To study the influence of rock glaciers on the hydrological regime (Haeberli, 1990; Haeberli et al., 1993; Burger et al., 1999; Brenning, 2005; Azocar and Brenning, 2010), field methods like drilling or geophysical prospecting are useful tools (Arenson and Jakob, 2010). This study quantitatively provides structural and physical parameters for the questions mentioned above and focuses on the lateral assessment of hitherto poorly or sparsely determined parameters, such as ice content, permafrost thickness, and depth to bedrock found below the surface debris layer.

Core drilling on rock glaciers (e.g. Haeberli et al., 2006; Tab. 1) showed that the internal structure and distribution of ice can change significantly in vertical and lateral direction (Barsch et al., 1979; Vonder Mühll and Holub, 1992; Arenson et al., 2002).

These authors describe layers composed of either massive ice, ice in pore space, ice lenses, or sandy-silty materials found below the active layer. The active layer consists of boulders (up to several meters in diameter) and fine-grained sandy-silty materials in the European Alps, and of gravel or cobbles in other regions (Isaksen et al., 2000). Recent core drilling at nearby Lazaun rock glacier, South Tyrol, Italy (Tonidandel et al., 2010) exhibits similar internal structures like distinct shear horizons as observed in earlier studies (e.g., Arenson et al., 2002). The permafrost core at Lazaun consists of a mixture of ice, sand and gravel with a thickness of ~ 17 m with ice-free layers composed of boulders and gravel. It rests on a lodgment till that is overlain by a similar layer of boulders (~ 5 m). The thickness of the lodgment till was > 7 m. Inclinometer data indicate that no significant displacements occur beneath the base of the ice-rich permafrost.

In the last decade various geophysical methods were applied in mountainous permafrost terrain (e.g. Vonder Mühll et al., 2001; Hauck and Vonder Mühll, 2003a; Kneisel et al., 2008) for mapping and exploring the internal structure of the permafrost and its temporal changes (Table 1). For structural investigation of rock glaciers, seismology, ground-penetrating radar (GPR) and geoelectrics are usually applied. Gravimetric measurements have been carried out rarely during the past years although they allow constraining the bedrock topography or ice content estimates. Recently, combinations of several geophysical methods provided improved models of rock glaciers (e.g., Vonder Mühll et al., 2000; Farbrot et al., 2005; Ikeda, 2006; Maurer and Hauck, 2007; Hausmann et al., 2007; Leopold et al., 2011) and facilitated the establishment of rheological models in order to benchmark the geophysical interpretations (Hausmann et al., 2007).

Ice contents of rock glaciers derived from borehole records or geophysical measurements range from 10 to almost 100 % and often vary significantly with depth (e.g. Potter, 1972; Barsch et. al., 1979; Francou et al., 1999; Haeberli et al., 2006; Hausmann et al., 2007). So far, ice content estimates based on geophysical methods are computed from either (i) seismic P-wave velocities using the Müller formula (Röthlisberger, 1972; Barsch, 1996), (ii) a density model based on gravimetric measurements (Hausmann et al., 2007), or (iii) seismic P-wave velocities and electrical resistivities using Archie's law (Archie, 1942) and an extended Timur equation (Timur, 1968; Hauck et al., 2011).

In this study, we describe the internal structure of Ölgrube and Kaiserberg rock glaciers based on ground-penetrating radar, seismic refraction, and gravimetric measurements. The resulting structural and physical parameters are used to discuss their relation to the dynamic behaviour of the rock glaciers. Therefore, we compare the two rock glaciers from this study and one additional rock glacier, which was investigated by applying the same methods in an earlier study (Hausmann et al., 2007), and draw conclusions that help to understand the internal structure of rock glaciers in general. The following questions are addressed: Does their creep behaviour follow the same principles, and can such a relation be formulated from the assessed parameters? Do the GPR-reflections correlate with the resulting structural and physical parameters?

2. Field sites

Both investigated rock glaciers are located in the catchment area of the Kauner Valley in the western Ötztal Alps, Tyrol,

Method		Reference
Geoelectrics		Evin et al., 1997; Croce and Milana, 2002; Vonder Mühll et al., 2000; Hauck et al., 2003; Ribolini et al., 2007
Ground-penetrating radar (GPR)		Isaksen et al., 2000; Lehmann and Green, 2000; Berthling et al., 2000, 2003; Degenhardt et al., 2002; Degenhardt and Giardino, 2003; Otto and Sass, 2006; Fukui et al., 2008; Monnier et al., 2008, 2011; Krainer et al., 2010; this study
Gravimetry		Klingele and Vonder Mühll, 1993; Vonder Mühll, 1993; Hausmann et al., 2007; this study
Seismology		Musil et al., 2002; Ikeda, 2006; Hausmann et al., 2007; this study
Application		**Reference**
Detection and Mapping		Hauck and Vonder Mühll, 1999, 2003b; Vonder Mühll et al., 2002; Hauck et al., 2004; Ribolini et al., 2007
Temporal changes		Hilbich et al., 2008, 2009; Hilbich, 2010
Internal structure [a]		Vonder Mühll et al., 2000; Farbrot et al., 2005; Musil et al., 2006; Ikeda, 2006; Maurer and Hauck, 2007; Hausmann et al., 2007; Leopold et al., 2011; Scapozza et al., 2011; this study
Ice content	Drilling	Haeberli et al., 1988; Vonder Mühll and Holub, 1992; Arenson and Springman, 2005a; Tonidandel et al., 2010
	Seismic velocities [b]	Röthlisberger, 1972; Barsch, 1996
	Density model	Hausmann et al., 2007; this study
	Seismic velocities and electrical resistivities [c]	Hauck et al., 2011

[a] from combinations of geophysical methods, [b] using the Müller formula, [c] using Archie's law (Archie, 1942) and an extended Timur equation (Timur, 1968)

Table 1: Compilation of representative studies of mountain permafrost using geophysical methods.

Austria (Fig. 1) and represent two of the largest rock glaciers in this area. They were chosen because of their large size, their impressive high front lobes, their high surface velocities (Finsterwalder 1928; Pillewizer 1957, Berger et al., 2004, Krainer et al., 2006), and their expected high ice volume. Additionally, many previous studies exist (Krainer and Mostler, 2002; Krainer et al., 2002; Krainer et al., 2007). Recent work on a regional rock glacier inventory exhibited 123 rock glaciers (7.3 km²) in the catchment of the Kauner Valley which include 39 (32 %) active, 42 (34 %) inactive and 42 (34 %) relict rock glaciers. At the closest meteorological station (Weißsee, 2540 m a.s.l, 4 km SW to Ölgrube) the mean annual air temperature is -0.4 °C for the period 2007-2009 and the annual precipitation is 1300 mm for the period 1980-2000.

2.1 Ölgrube

The rock glacier Innere Ölgrube (46.8945° N, 10.7539° E) is located in a small west-trending tributary valley of the Kauner Valley in the western Ötztal Alps. The bedrock in the catchment area consists of orthogneiss, paragneiss and mica schist of the Stubai-Ötztal complex (Hoinkes and Thöni, 1993). The rock glacier, which is composed of two tongue-shaped parts, is 250 m wide and 880 m long and terminates on the relatively flat ground of an alpine meadow at an altitude of about 2380 m (Figs 1a, b). The rock glacier covers an area of 0.2 km², the drainage area measures 1.9 km² (including a small cirque glacier covering 0.15 km²). The surface of the northern part of the rock glacier shows distinct longitudinal and transverse furrows and ridges. It is composed of debris derived from orthogneiss of the Ölgrubenspitz massif. The active front is approximately 70 m high and 40 - 45 ° steep. The surface material of the active layer generally consists of two horizons: a very coarse-grained surface layer which is underlain by a finer-grained layer. The coarse-grained debris mantle shows an average grain size of the a-axis of 20 - 40 cm, but individual blocks reach maximum diameters up to several meters (Berger et al., 2004). The finer-grained layer, which is exposed at the steep sides and the frontal slope, consists of sandy silt to silty sand with embedded boulders.

The ground temperature in the debris layer shows a distinct pattern of seasonal and diurnal variations. During winter, temperatures at the base of the snow cover are significantly lower on the rock glacier than outside, indicating the presence of permafrost (see Berger et al., 2004).

Discharge shows distinct seasonal and diurnal variations. Electrical conductivity is very low during high discharge peri-

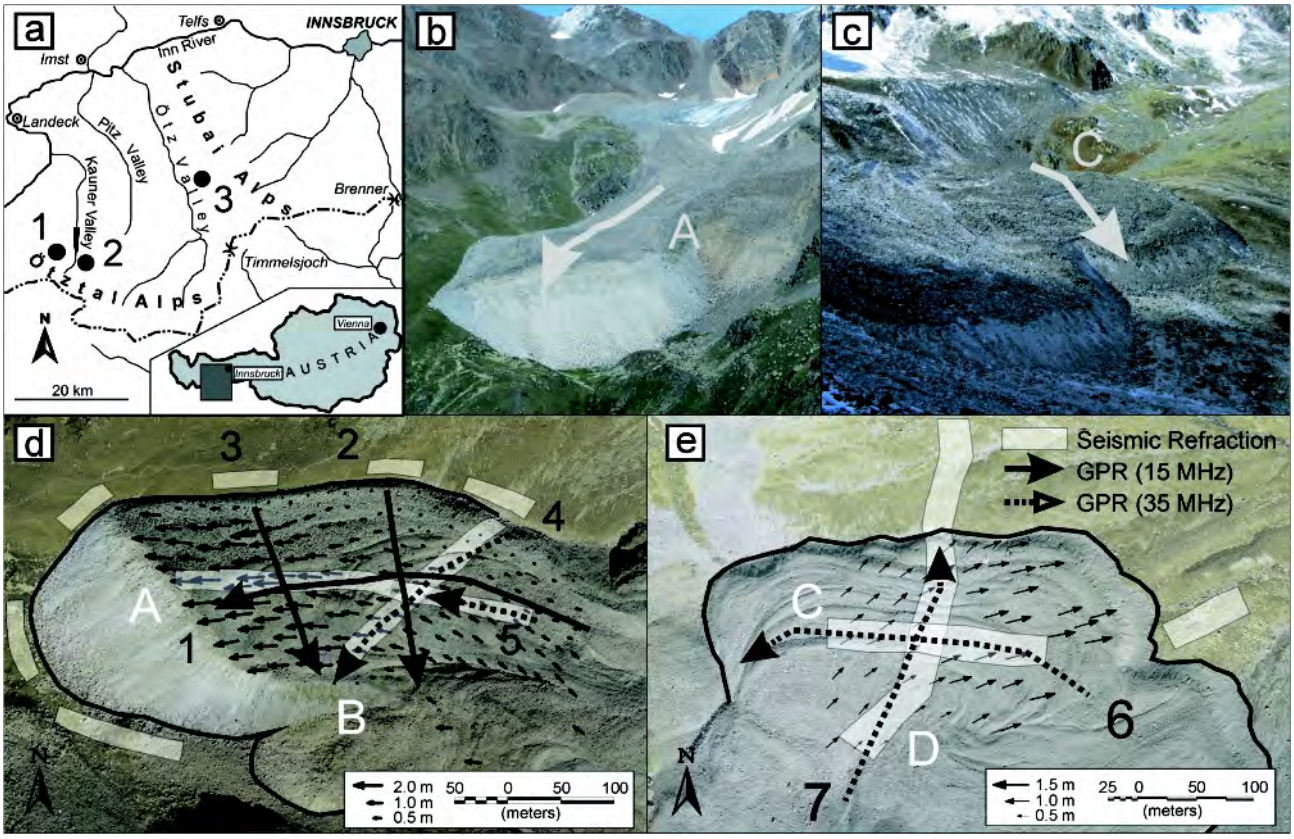

Figure 1: Location map, photographs and location of profiles of the two studied rock glaciers. (a) Location map of the rock glaciers Kaiserberg (1), Ölgrube (2), and Reichenkar (3). (b, c) Photographs of the rock glaciers Ölgrube (b, d) and Kaiserberg (c, e) with the flow direction and the locations of the discussed profiles. (d, e) Aerial photographs of the Ölgrube and Kaiserberg rock glaciers with the displacements and the locations of the geophysical investigations. The displacements were measured in 2003 and 2004 (381 days) at Ölgrube and in 2002 and 2004 at Kaiserberg (750 days). Ground-penetrating radar (GPR) profiles and locations of the seismic stations are highlighted by black arrows and white regions. The letters A-D denote the main seismic profiles and the numbers 1-7 the GPR profiles on the rock glacier. Aerial photographs are from 2003 and reproduced by permission of the Administration of Tyrol/tiris.

ods with typical values of 25 – 45 µS/cm. Towards autumn, when discharge decreases, electrical conductivity increases to values of 110 – 130 µS/cm. The water temperature of the rock glacier springs remains permanently < 1.5 °C during the entire melt season. Detailed data concerning hydrology are presented by Berger et al. (2004), Krainer and Mostler (2002), and Krainer et al. (2007).

The earliest measurements of surface velocities were reported by Finsterwalder (1928). For the period 1923 - 1924, displacements up to 0.5 m were observed. Pillewizer (1957) measured values of 0.5 m/a along a profile on the lower part and 0.75 m/a along a profile on the upper part of the rock glacier for the period 1938 - 1957. Real-Time Kinematic GPS measurements have been started in the year 2000 by using 21 survey markers along two profiles and 2 reference points outside the rock glacier (Krainer and Mostler, 2006). Additionally, 165 survey markers from the gravimetric measurements were observed in 2002 and 2003. The highest surface velocities (up to 2.5 m/a) were measured near the front, velocities gradually decreased upward, referring to an extensional flow regime. In the upper part the highest surface velocities (0.95 m/a) occurred near the southern margin and decreased towards the northern margin of the northern rock glacier. Surface velocities generally increased from 2002 to 2004, but decreased in 2005 (details in Krainer and Mostler, 2006) which is in accordance to other rock glaciers in the European Alps (Delaloye et al., 2008).

2.2 Kaiserberg

The Kaiserberg rock glacier (46.9109° N, 10.6769° E) is located in the upper reaches of the east-facing Kaiserberg Valley, which is a tributary of the Kauner Valley. The rock glacier has a lobate form with a maximum width of 550 m, and lengths ranging from 350 to 400 m. The rock glacier covers an area of 0.15 km². The frontal slope at an altitude of 2585 m is active and steeply inclined (41 - 45 °). The coarse-grained surface layer shows pronounced ridges and furrows. Melt water is released at two springs at the foot of the steep front. The rock glacier is predominantly composed of orthogneiss clasts, subordinated are mica schist and amphibolite clasts.

The grain size of the surface layer varies from place to place. Grain size measurements (Berger, 2002) show that clasts with grain sizes of 1 - 20 cm dominate on fine-grained areas, boulders > 50 cm are rare (max. 4 %). On coarse-grained areas the average grain-size is 40 - 55 cm. 35 % of the boulders are > 50 cm, 6 % > 100 cm, the maximum size is 537 cm. Samples taken at the steep front of the finer-grained layer contain 4 – 6 wt% clay and silt, 4 – 5 wt% sand, and 90 wt% pebbles and boulders. The sorting is extremely poor.

The BTS (bottom temperatures of the snow cover) recorded on the rock glacier were always lower than those measured outside the rock glacier (Berger, 2002).

At the Kaiserberg rock glacier 112 survey markers were installed on the rock glacier and 2 reference points outside. The markers were first measured in 2002 and re-measured in 2004. The highest surface velocities were determined at the steeper eastern part of the rock glacier. Surface velocities were > 1 m/a, the highest values being 2.0 m/a. Markers located at the central and western part of the rock glacier yielded displacements of 0.4 - 0.9 m within a period of two years (Krainer and Mostler, 2006).

3. Methods

3.1 Geophysical investigation approach

In this study we follow the concept introduced by Hausmann et al. (2007) to investigate the internal structure of ice-rich rock glaciers:

1. GPR measurements provide information on the depth to the base of the ice-rich permafrost and locally to the bedrock.
2. Seismic refraction provides information on the depths to the ice-rich permafrost and to the surface of the bedrock. With the seismic data and the knowledge of GPR it is clear that the following 4 layers have to be resolved: a) surface debris layer (“active layer”), b) ice-rich permafrost body, c) unfrozen (ice-free) sediments below the permafrost body, and d) the surface of the bedrock. As the sediment layer is a lower velocity zone, it can not be determined by seismic data alone. The necessary additional information is provided by GPR and P-wave velocities of the surrounding sediments. A confirmation of this approach is found in areas where the bedrock surface is resolved by GPR and seismic refraction. As we focus during the seismic analysis on deeper parts of the rock glacier, the surface debris layer, with grain sizes varying from fine to coarse, is resolved as one layer.
3. The results from GPR and seismic refraction are combined to establish a density model. The density (porosity) for the surface debris layer and the sediment layer below the permafrost is calculated from a relationship between P-wave velocity and porosity (Watkins et al., 1972). In a next step the density of the ice-rich permafrost is determined by the gravimetric data. Based on the derived structure and densities, the relative ice content is calculated (Hausmann et al., 2007).

In this study we additionally use the resulting structural and physical parameters to better understand the dynamic behaviour of the rock glacier. To quantify the stress regime which drives the movement of the rock glaciers, we compute a parameter related to the shear stress at the base (Paterson, 1994) of the ice-rich permafrost layer. In a next step we compare this parameter with the observed parameters (P-wave velocities, bulk densities, thicknesses) from the two rock glaciers and one rock glacier that was investigated by applying the same methods (Hausmann et al., 2007). To describe the movement of the three rock glaciers we use the power law. Finally, the GPR-reflections of the permafrost layer are displayed together with the P-wave velocities, the densities (ice contents) and the surface velocities along the profiles of the main flow direction.

3.2 Data acquisition and processing

Ground-penetrating radar data were collected using a GSSI SIR 2000 system in combination with the multiple low-frequency antennae of 15 and 35 MHz. All measurements were conducted in the same season when the rock glaciers were covered with a thick layer of snow and when melt water was absent. Figures 1d and e display the location of the recorded profiles at Ölgrube rock glacier for the years 2002 (profiles 4 - 5; 35 MHz) and 2007 (profiles 1 - 3; 15 MHz). At Kaiserberg a longitudinal and a transverse profile (6, 7) were surveyed in 2002 using the 35 MHz antennae. The data were acquired along longitudinal and transverse profiles using a fixed antenna spacing of 4 m and a spatial sample interval of 1 m (point modus). The main recording parameters were 900 ns (35 MHz) or 1200 ns (15 MHz) record length, 1024 samples per scan, 16 bits per sample, and 32-fold vertical stacking. Vertical resolution defines how far apart two interfaces must be in order to appear as separate reflectors. An electromagnetic pulse of 15 MHz propagates with a wavelength of 9 m in ice-rich permafrost (assuming a wave speed of 0.14 m/ns), which results in a vertical resolution of about 2.3 m (¼ of the signal wavelength; Yilmaz, 2001). However, the presence of thin intermediate layers in the permafrost with a large contrast in permittivity (e.g., shear zones) can be well identified (e.g., Maurer and Hauck, 2007; Krainer et al., 2010), whereas the thickness can not be resolved without wavefield modelling (Yilmaz, 2001). The raw data were processed with trace mixing (reduction of antenna noise), automatic gain control (300 - 500 ns length), trapezoid band pass-filter for the 15 MHz (8-10-40-45 MHz) and 35 MHz records (5-15-45-70 MHz), deconvolution, migration, and static corrections using the 2D software ProMAX (Landmark). For the migration we applied the Steep dip explicit Finite-Difference (FD) time migration algorithm with a maximum dip of 70°. Electromagnetic (EM) wave speed was assessed by both reflection hyperbolae identified in the radargram sections and migration velocity analyses. The latter one provides an accurate interval velocity model for the depth migration. The derived wave speeds are 0.14 m/ns for Ölgrube and 0.15 m/ns for Kaiserberg. Since unshielded antennae were used, all discussed features are carefully examined with regard to their possible origins (e.g., reflections from rock walls). To get an overview on the spatial connection of identified reflectors, we displayed the data within the three-dimensional (3D) view of the software GoCAD (Earth Decision/Paradigm).

Seismic refraction measurements were carried out for Ölgrube along the profiles A and B (Fig. 1b, d) in summer 2003. The seismic survey at Kaiserberg was carried out in June 2002 by stations arranged along the profiles C and D (Fig. 1c, e). A layout with shots and receivers deployed on the rock glacier (along a longitudinal and a transverse profile) and beside the rock glacier was used. The average spacing of the geophones (4.5 Hz natural frequency) on the rock glacier was about 15 m and on the nearby sediment layer between 15 and 200 m. The layout for Ölgrube additionally includes stations arranged outside the rock glacier on ground composed of sediment to provide a sparse 3D-aspect. Details on the shot and receiver layout are shown together with the data (Fig. 4). The seismic measurements were carried out using 44 shots for Ölgrube, 37 shots for Kaiserberg and 30 single channel miniature recorders (Reftek 125). Seismic energy, generated by the use of detonating cords blasted at the surface, was recorded simultaneously by all receivers. The temporal sample interval was 1 ms.

The raw data were processed with trace Direct-Current (DC) removal, bottom mute, trapezoid band pass-filter (10-30-140-180 Hz) and constant gain control for Kaiserberg rock glacier, and with bottom mute and constant gain control for Ölgrube rock glacier. To provide an estimate of a 1D-layer model, we employed a plot of first arrival travel times and a stack of traces to offset bins of 6 m with geophones and shots on the rock glacier (Hausmann et al., 2007). The depth to the ice-rich permafrost is computed via shot- and receiver-based delay times using the refraction statics calculation tool in ProMAX. The calculation of the depth to the bedrock takes advantage of the 3D-aspect of the shot and receiver layout and is computed by a 3D inversion (e.g., Kirchheimer, 1988a, 1988b) in which delay times are proxies for refractor depths (Telford et al., 1990).

For gravity field survey a total of 230 stations were measured at Ölgrube in summer 2003 and, respectively, 130 stations at Kaiserberg in July 2002. A Scintrex CG-3 gravity meter (accuracy: ±10 µGal; 1 µGal=10^{-8} ms^{-2}) was used to make measurements on the rock glaciers and at adjoining locations in order to estimate the regional field. At Ölgrube 187 locations on the rock glacier and 43 beside it were measured (inlet in Fig. 5a). The average spatial sample interval for stations situated on the rock glacier was ~ 20 m. For Kaiserberg 130 locations were measured at the rock glacier and 25 outside (see inlet in Fig. 5b). The spatial sample interval for stations situated on the rock glacier was ~ 25 m. The positions of the stations were determined by RTK-GPS (accuracy of elevation: ± 6 cm). Instrument drift was recorded by repeated measurements at a base station and corrected linearly.

The Bouguer anomaly is computed after applying reductions for: the instrument drift, the atmosphere, the normal gravity of the ellipsoid, the height dependency (free-air reduction), and the crustal mass (topographic correction and Bouguer plate). Corresponding to a regional density map (Granser et al., 1989), a value of 2670 kg/m^3 was used for the mass correction for both locations. For the topographic reduction we used the algorithm by Götze and Lahmeyer (1988) and the official Austrian DTM (raster size: 50 m) in combination with all locations that were surveyed by RTK-GPS, a reduction radius of 50 km, and a constant density value. In the next step a linear regional trend is subtracted using only stations beside the rock glaciers. Subsequently, the residual anomaly was interpreted by 2.5-D density modelling using the software GMSys (Geosoft, Oasis Montaj). The density model is constrained by (a) the structural model and (b) a conversion of seismic velocity to density for the surface boulder layer and the sediment layer below the permafrost. The dependence of in-situ compressio-

nal wave velocity on porosity in unsaturated rocks was investigated by Watkins et al. (1972) and suggests a logarithmic relationship between P-wave velocity and porosity:

$$\phi = -0.175 \cdot \ln(v_p) + 1.56 \quad (1)$$

Equation (1) shows the least square regression where Φ is the fractional porosity and v_p the seismic P-wave velocity.

4 Field results

4.1 Ground-penetrating radar

For the Ölgrube rock glacier the migrated radar sections exhibit the following main reflectors for the longitudinal profile

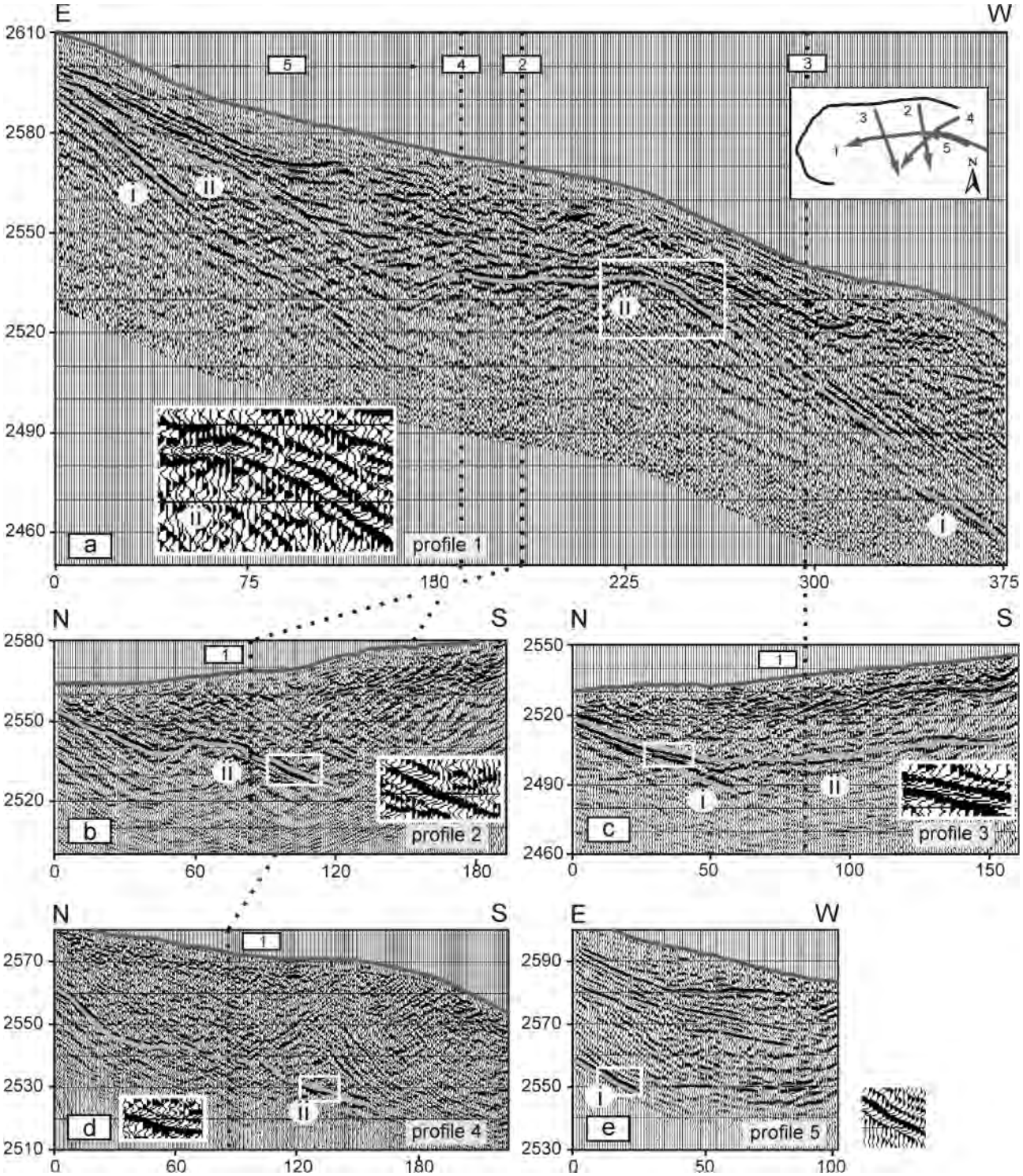

Figure 2: Migrated ground-penetrating radar sections along the Ölgrube rock glacier. Interpretations are superimposed on the section: (i) high-amplitude basal reflector, (ii) pronounced internal reflector identified in 4 of 5 sections. For the locations of the profiles see the inlet in the topmost section. The present flow direction is from E to W.

(profile 1, 375 m long and profile 5 as part of this profile) (Fig. 2a, e): (i) a high-amplitude basal reflector dipping from 0 to 60 m, (ii) a pronounced internal reflector ranging from 0 to 100 m and from 155 to 275 m. In the transverse profile 2 (Fig. 2b) only the pronounced reflector (ii) was identified. At the northern margin of the rock glacier the reflector has a depth of ~ 7 m and dips towards the southern part to a depth of ~ 30 m. The pronounced reflector (ii) is displayed again in the transverse profile 3 (Fig. 2c). It appears almost continuously along the whole profile and, as before, dips from north to south. The maximal depth of the reflector is about 30 m. The second reflector was determined from 25 to 60 m and is assigned to the basal reflector (i). Transverse profile 4 (Fig. 2d) again shows the continuation of reflector (ii) which dips from the northern part (~ 20 m) to the southern part (~ 40 m). Part of the high-amplitude basal reflector (i) is identified from 0 to 35 m in the longitudinal profile 5 (Fig. 2e). The data depict a pronounced internal reflector (ii) that appears almost continuously along all profiles. This reflector can be identified in four profiles (1-4) and is interpreted as an ice-free sediment layer. This is indicated as follows: The reflector can be identified clearly and is continuous over a large extent of the investigated area. It causes a high reflectivity that is compatible with wet and/or fine-grained sediments. In the area next to the rock glacier boundary, the surface of the reflector shows a similar curvature as the ice-free sediment layer outside the rock glacier. It is not compatible with the bedrock surface shown by seismic refraction and gravimetry presented in the next sections.

For Kaiserberg rock glacier the location of the two profiles and the migrated radar sections are displayed in Figure 3. Similar to Ölgrube rock glacier, we identified two main reflectors: (i) a basal reflector and (ii) an internal reflector. Starting with profile 7, the basal reflector (i) is clearly identified at the southern part (0 - 80 m). Towards the north it declines to a

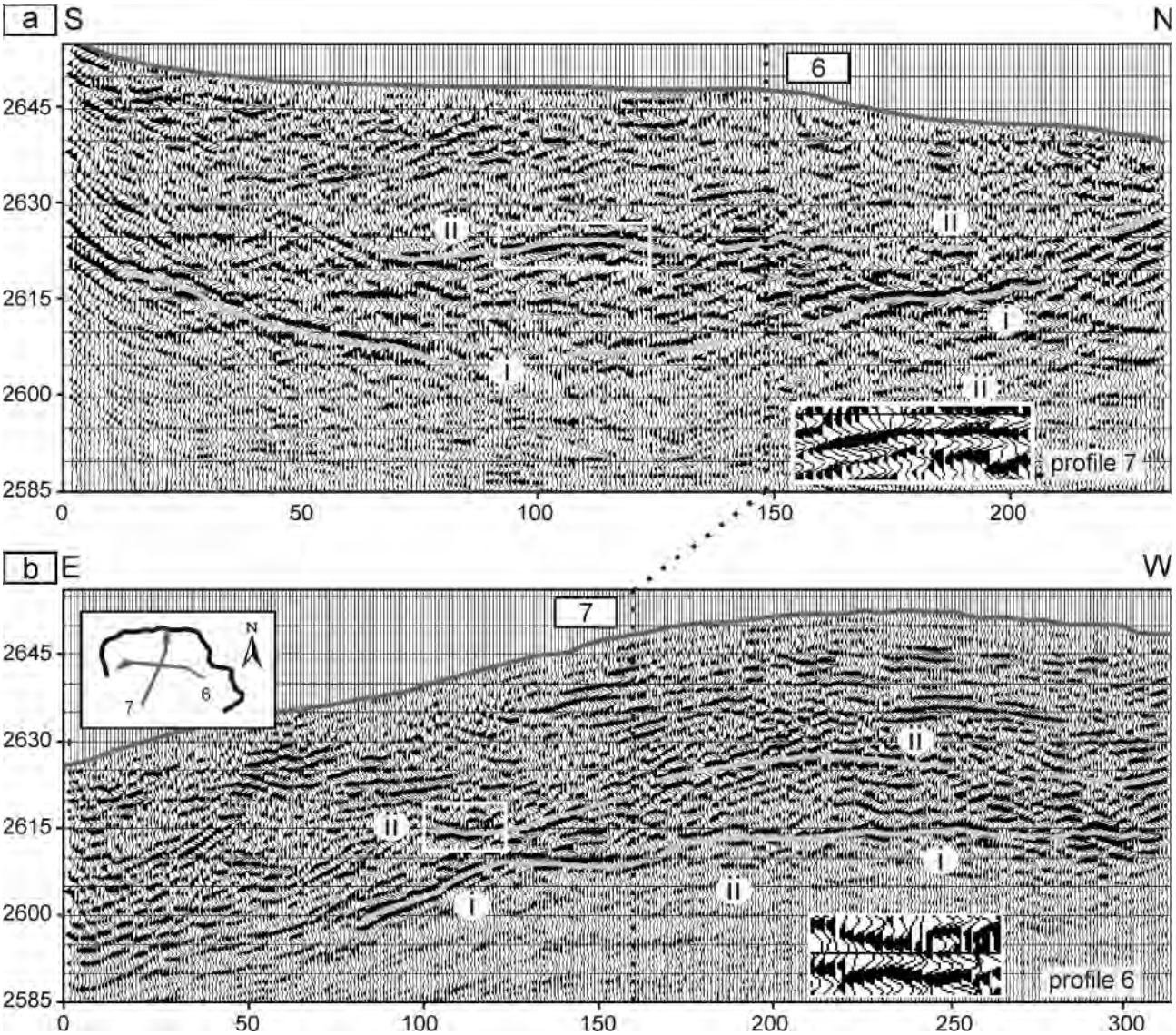

Figure 3: Migrated ground-penetrating radar sections along the Kaiserberg rock glacier. Interpretations are superimposed on the section: (i) high amplitude basal reflector, (ii) pronounced internal reflector identified in all sections. For the locations of the profiles see the inlet in the topmost section. The present flow direction is from W to E.

depth of 45 m and is identified again at a profile distance of 160 - 210 m. The continuation of this reflector is shown in profile 6. In this section the reflector is clearly identified between 80 and 160 m and to some extent from 160 m to 310 m. The correlation of these two reflectors is strengthened since the interpolated reflector from profile 7 (140 - 160 m) is connected at an elevation of 2610 m with the reflector of profile 6. Noticeable is the abrupt termination of high-amplitude reflections below this reflector. The internal reflector (ii) is well identified from 100 to 250 m and stepwise from 270 to 310 m. The reflector separates a zone of reflectors parallel to the surface with a zone of undulating and chaotic reflections. In profile 7 the internal reflector is clearly identified from 70 to 170 m. At the northern part of profile 7 the high amplitude reflector (i) lies at an elevation of ~ 2620 m. The seismic data recorded to the north of the rock glacier (see next section) show similar values for the altitude of the bedrock interface.

4.2 Seismic refraction

For the Ölgrube rock glacier representative seismic data are displayed in Figure 4a. It shows a seismogram with all traces of geophones and shots on the rock glacier stacked to offset bins of 6 m width. Both the stack and the travel times (not shown) resolve three layers. Correlation of the different phases lead to an estimate of the P-wave velocities for each layer: surface boulder layer - 710 m/s, ice-rich permafrost - 3430 m/s, and bedrock - 4500 m/s. To compute the depths to the ice-rich permafrost, we used 474 first arrivals with offsets ranging from 30 to 160 m. Depths range between 3 m and 8 m, with an average of 5.2 m. The P-wave velocity for the ice-rich permafrost refracted wave resulted in a mean value of 3195 ±175 m/s for profile A and 3085 ±105 m/s for profile B (see inlet in Fig. 4a). The bedrock refractor depths were calculated by the inversion of 378 travel times. The refractor velocities were determined with a value of 4460 ±50 m/s and are attributed to the velocity of jointed gneiss. Prior to the calculation of the depths down to bedrock, we had to consider the additional delay time caused by the ice-free sediment layer below the permafrost. Therefore, we investigated the travel times of all refracted waves that were generated and recorded outside of the rock glacier. The travel times clearly show two layers with a velocity of 800 - 1350 m/s (for short and large offsets) for the ice-free sediments and ~ 4500 m/s for the bedrock. Computed depths to bedrock were 15 - 20 m. The highest depths occur near the north-western margin of the rock glacier where a rampart is mapped (K. Krainer, unpublished data). The final depths to the bedrock were calculated by using a velocity of 1350 m/s for the ice-free sediments below the permafrost. This value corresponds to compacted sediments (Hauck and Kneisel, 2008) and was observed at larger offsets. Beneath the rock glacier the mean depth to the ice-free sediments is 34 m and to the bedrock 46 m.

For the Kaiserberg rock glacier the seismic data are shown in Figure 4b. The correlation of the different phases exhibits a composition similar to Ölgrube and leads to an estimate of the P-wave velocities for each layer: surface debris layer - 1080 m/s, ice-rich permafrost - 3600 m/s, and bedrock - 4550 m/s. To compute the depths to the ice-rich permafrost, we used 404 first arrivals with offsets ranging from 30 to 150 m. Depths range between 2 m and 8 m, with an average of 5.4 m. The P-wave velocity for the ice-rich permafrost refracted wave resulted in a value of 3675 ±323 m/s for profile C and 3120 ±218 m/s for profile D.

The bedrock refractor depths were calculated by the inversion of 350 travel times. The refractor velocities were determined by the value of 4120 ±290 m/s and are attributed to the velocity of jointed gneiss. Outside of the rock glacier the travel times clearly show two layers with a velocity of 800 - 1250 m/s for the ice-free sediments and ~ 4500 m/s for the bedrock. Calculated depths to bedrock were 12 - 18 m, the highest depths occur near the northern margin of the rock glacier. The final depths to the bedrock were calculated by the use of a velocity of 1250 m/s for the ice-free sediments. Under the rock glacier the mean depth to the ice-free sediments is 28 m

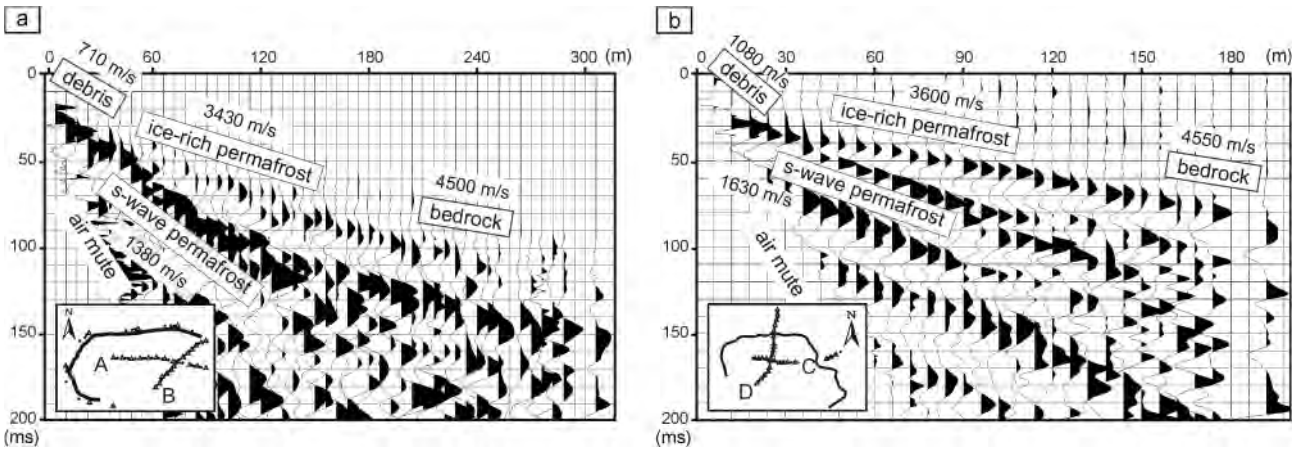

Figure 4: Data from the seismic surveys on the Ölgrube (a) and Kaiserberg (b) rock glaciers: Representative seismic data are displayed as offset bin stacks with interpretation of the recorded signals. For the stack, all traces with geophones and shots placed on the rock glaciers were stacked to offset bins of 6 m width. For the locations of the surveys see the inlets.

and to the bedrock 37 m.

4.3 Gravimetry

For the Ölgrube rock glacier the subtraction of the regional trend leads to a pronounced residual Bouguer anomaly (Fig. 5a). The residual field exhibits two anomalies. The larger one (-1.4 mGal) is located at the eastern part of the rock glacier, indicating a density decrease within the rock glacier. The two anomalies are separated by a zone of higher anomaly values (-0.5 mGal) that is directed from N to S. Northwards of the rock glacier (in prolongation of the described zone) a bedrock outcrop can be observed. Below this zone we also identified a pronounced GPR reflector (profile 350 in Fig. 2). The smallest value for the depth of this reflector is found in this zone.

For the Kaiserberg rock glacier the subtraction of the regional trend leads to a clear residual Bouguer anomaly (Fig. 5b) with its minimum (-0.8 mGal) located at the northern part of the rock glacier.

5 Integrated geophysical models

In this section we integrate the results from the three applied geophysical methods to display the structure, to provide a density model, and finally to estimate the ice content of the two rock glaciers. The integrated models (Fig. 6, 7) are presented for each rock glacier separately and are established along the seismic profiles A and C (Fig. 1b,c). We describe how the density model is parameterized and subsequently focus on the interpretations. Representative values of the resulting structural and physical parameters are summarized in Table 2.

5.1 Ölgrube rock glacier

For Ölgrube we display the structure with the density model along the sections A and B (Fig. 6). The surface debris layer is well-defined by the seismic refraction. The top of the ice-free sediment layer below the permafrost body is derived by the prominent internal GPR reflector. This layer can be extended to the visible sediment layer beside the rock glacier. The bedrock surface under the rock glacier follows the result from the seismic refraction and corresponds to the basal GPR reflector. Additional constraints from the basal GPR reflector and the seismic investigations beside the rock glacier are used to continuously delineate the bedrock surface. With constraints from the structure and the densities converted from the seismic velocities using the relation of Watkins et al. (1972), we established the density model by varying the density of the permafrost layer. We introduce a value of 1604 kg/m³ for the surface debris layer and 1870 kg/m³ for the ice-free sediments below the permafrost. The model was fit to the observed gravimetric data using values between 1410 to 2150 kg/m³ for

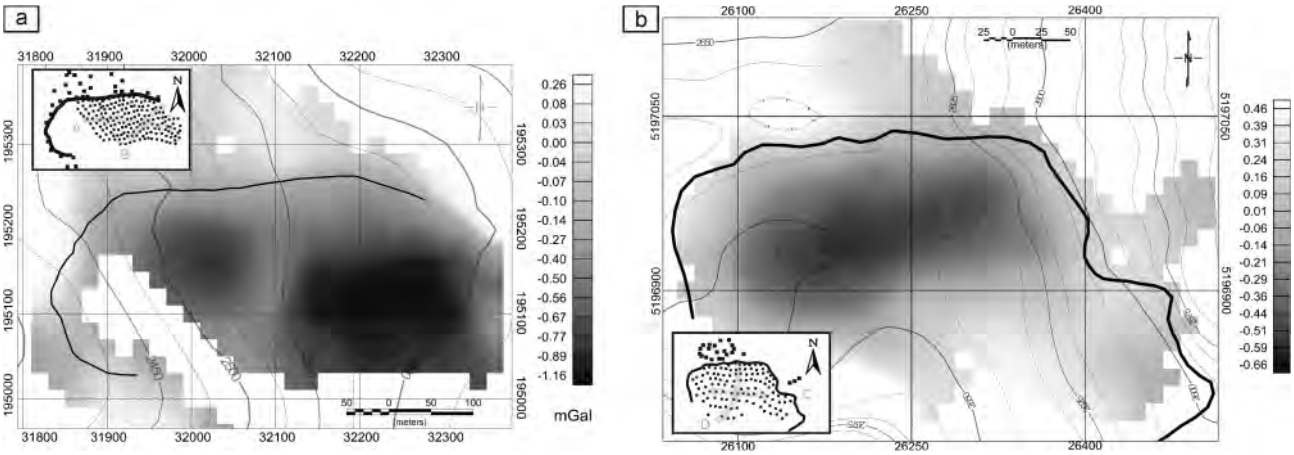

Figure 5: Data from gravimetric surveys on the Ölgrube (a) and Kaiserberg (b) rock glaciers: The data display the residual Bouguer anomaly. For the locations of the surveys – each dot represent a single measurement – see the inlets.

	profile	v_{GPR} (m/ns)	v_P (m/s)	d_{pf} (kg/m³)	d_{boul} (kg/m³)	dh_{boul} (m)	dh_{pf} (m)	H_{bed} (m)	I (%)
Ölgrube (front area)	A		3091	1940		5.3	31	50	43
Ölgrube (root area)		0.14	3272	1620	1604	4.6	27	46	61
Ölgrube	B		3085	1920		5.1	25	44	44
Kaiserberg	C	0.15	3675	1950	1770	5.4	23	38	41
Kaiserberg	D		3120	1850		4.4	20	37	47

Table 2: Structural and physical parameters as obtained from the geophysical models. For the list of abbreviations see Appendix A.

the permafrost layer. The model residuals range between ±28 µGal. Note that our methodology requires to describe a 4-layer model from the observed data. At locations where the bedrock surface could be determined by GPR and seismic refraction, the results show that a 4-layer model with an ice-free sediment layer prevails. BTS measurements (section 2.1; Berger 2002; Berger et al. 2004) and seismic refraction indicate permafrost-free ground beside the rock glacier. The ice content was estimated on the basis of a two phase model (ice, debris) using the derived densities from the model and the measured bulk density of the embedded rock (2690 kg/m³). The rock density was derived from buoyancy measurements on samples from the debris layer. The calculated volumetric values for the ice content vary between 31 and 72 % (Tab. 2).

The transverse profile B (Fig. 6a) images a distinct change in the direction of the valley floor (for the ice-free sediments and the bedrock) at a profile distance of about 100 m. It dips with a slope of 11 ° towards SW and lies in prolongation of an ice-free sediment layer (mainly lodgment till) and a bedrock outcrop at the front of the southern margin of the rock glacier. The profile shows higher densities and lower thicknesses of the permafrost layer towards N, which is in agreement with the lower surface velocities at this part of the rock glacier (see discussion).

The longitudinal profile A (Fig. 6b) runs parallel to the flow direction and images a pronounced bedrock threshold ranging from 250 - 350 m. Two bedrock outcrops close to the southern and northern margin of the rock glacier follow this trend. Our interpretation is strengthened by the clear reflector obtained by GPR and the gravimetric model that requires such a high-density structure (> 2500 kg/m³) at this location. Towards the eastern side of the rock glacier, the bedrock derived from seismic refraction and GPR data follows the same trend and rises up. This trend is also supported by a bedrock outcrop at the north-eastern margin of the rock glacier. In the centre of the profile, a zone of steeper surface slope is shown. According to the resolved structure, this zone is caused by a steeper permafrost base and obviously results in a thinning of the permafrost layer. This finding is similar to the flow of ice masses (Paterson, 1994). The thickness of the ice-free sediment layer below the permafrost does not change significantly below and in front of the rock glacier where the thickness was also determined (by a 2-layer model). The lowest densities occur at the eastern part and under the front of the rock glacier. In general a trend of increasing values for the density and the surface velocities is registered towards the front. Thus,

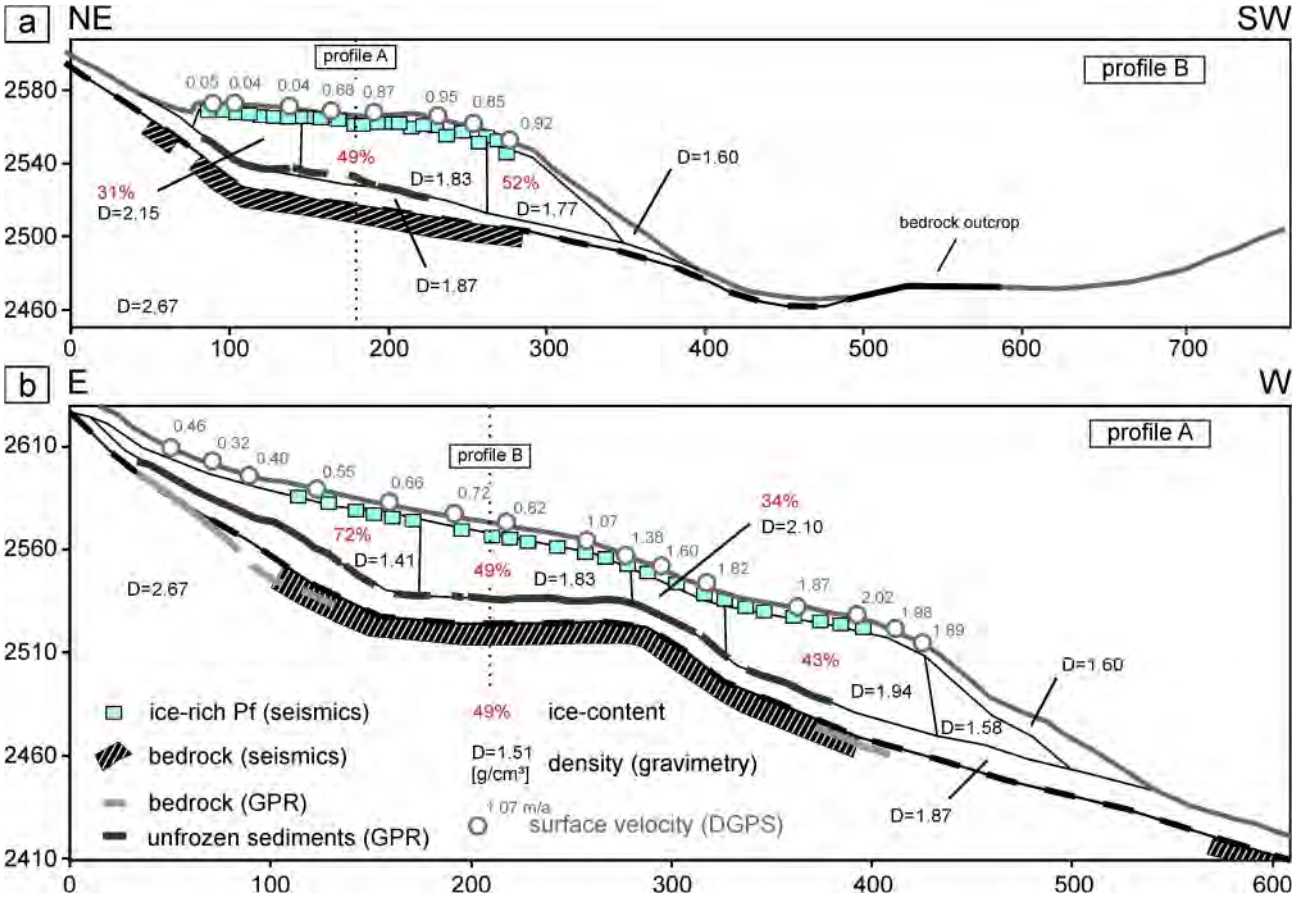

Figure 6: The geophysical model of Ölgrube rock glacier determined from the integrated methods ground-penetrating radar, seismic refraction, and gravimetry: (a) transverse section along the seismic profile B, (b) longitudinal section along the seismic profile A. The model presents a structural image of the rock glacier with the density distribution and an estimate of the ice content. Mean annual surface velocities during the period 2002 to 2004 are displayed along the flow direction.

the stated values for the structural and physical parameters were separated into a frontal part and a rooting zone of the rock glacier (Tab. 2).

5.2 Kaiserberg rock glacier

To derive the structure for the Kaiserberg rock glacier (Fig. 7), we use the same approach as described above. The density model was defined by values of 1770 kg/m³ for the surface debris layer and 1840 kg/m³ for the ice-free sediments below the permafrost. The existence of the ice-free sediment layer below the permafrost body is again constrained by the two main GPR reflectors and the depth to the bedrock. BTS measurements (section 2.2) and seismic refraction clearly indicate permafrost-free ground beside the rock glacier. The determined values for the ice-rich permafrost range from 1410 to 2190 kg/m³. The misfit of the density model was ±31 µGal for profile C and ±38 µGal for profile D. The ice content was estimated by using the measured bulk density of 2710 kg/m³ from buoyancy measurements on samples of the debris layer. The calculated volumetric values vary between 27 and 72 % (Tab. 2).

At profile D the resolved structure (Fig. 7a) images an increase in the thickness of the surface debris layer towards the northern front of the rock glacier. The trend of the bedrock follows the valley floor and dips slightly towards south until a steep wall is towered up. Our interpretation is strengthened by that part of the valley floor, where the bedrock follows the trend derived from seismic refraction and GPR. Along the profile, both the density and the thickness of the ice-rich permafrost decrease towards N. The basal structure does not support the idea of rock glacier creep along this profile. Despite the formation of major lobes (from N to S) the recent flow field (Krainer and Mostler, 2006) exhibits that the flow direction is exclusively directed towards E (along profile C). Both the moderate surface slope (< 2.5 °) and the fact that no trend for the permafrost base is imaged, constrain the development of actual creep processes along profile D.

For profile C, which runs parallel to the recent flow direction, the thickness of the surface debris layer does not change significantly (Fig. 7b). Beneath the rock glacier the trend of the bedrock runs parallel to the surface topography. Thicknesses of the ice-free sediment layer in the front of and beneath the rock glacier do not change significantly. In the central part of the profile, the bedrock derived from seismic refraction and GPR follows again the same trend. Only at the western part of the profile the trend of the bedrock is poorly defined. A high

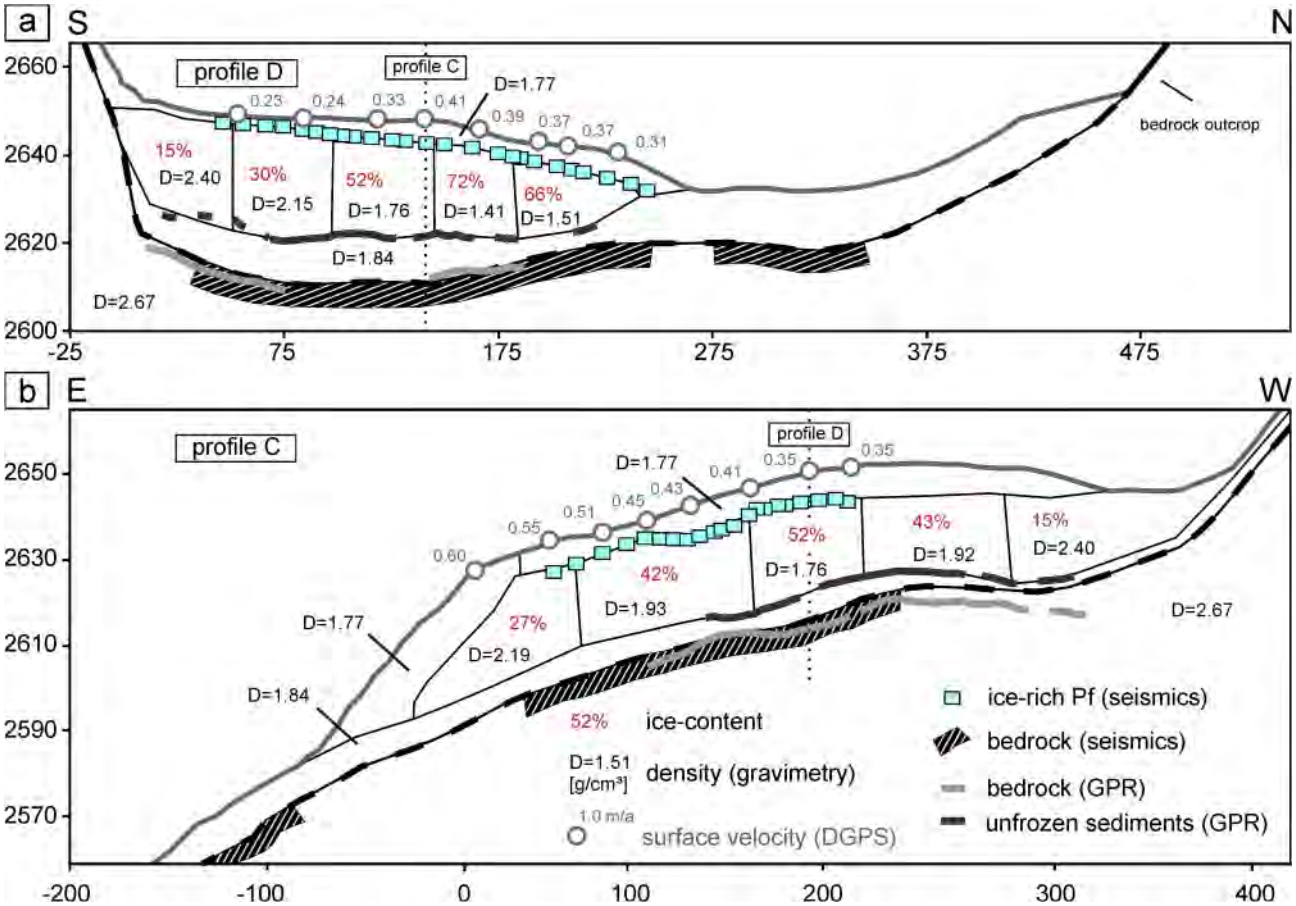

Figure 7: The geophysical model of Kaiserberg rock glacier as determined from the integrated methods ground-penetrating radar, seismic refraction, and gravimetry: (a) longitudinal section along the seismic profile D, (b) transverse section along the seismic profile C. The model presents a structural image of the rock glacier with the density distribution and an estimate of the ice content. Available mean annual surface velocities between 2002 and 2004 are also displayed along the flow profile.

value in the density model (2400 kg/m³) indicates a rise of the bedrock in this part. The mean values for the thickness and the densities of the ice-rich permafrost show only small changes (Tab. 2). In contrast to the other profile, the idea of creep is supported by the resolved structure. This can also be observed from the recent flow field.

6 Discussion

In this section we discuss if the structural and physical parameters that were obtained in this study correspond to the dynamic behaviour of the rock glaciers. We further look for a common relation that explains the creep behaviour on the basis of the resolved structure for the two investigated rock glaciers and an additional rock glacier named Reichenkar rock glacier (Hausmann et al., 2007; for location of this rock glacier see Fig. 1a). To understand the internal structure of rock glaciers in general, we further analyze and discuss the GPR-reflections of the permafrost layer and their relation to the obtained parameters.

Structural and physical parameters of rock glacier models should be related to their dynamic behaviour, especially creep. In Table 3 we compiled relevant parameters along longitudinal profiles of the two rock glaciers and the central longitudinal profile of the Reichenkar rock glacier (Hausmann et al. 2007). Along these profiles, surface velocities are known (section 2; Krainer and Mostler, 2006). The model of the Reichenkar rock glacier was determined by the same geophysical methodology as applied in this study.

Shear stress at the base of the permafrost layer of a rock glacier may serve as a characteristic quantity for the stress regime that drives the movement of the rock glacier. For an infinite plane layer of constant thickness h (measured in the vertical direction), average density *d*, and inclination *α*, the basal shear stress $\hat{\tau}_b$ is

$$\tau_b = d \cdot g \cdot h \cdot \cos(\alpha) \cdot \sin(\alpha) \qquad (2)$$

with *g* being the gravity acceleration. The calculation of the total thickness *h* and the average density *d* of the rock glaciers at each location is straightforward using the data from

	χ (m)	α (-)	dh_{bowl} (m)	dh_{pf} (m)	d_{pf} (kg/m³)	d_{bowl} (kg/m³)	v_p (m/s)	H_0 (m)	$H_{0,red}$ (m)	v_{surf} (m/a)	ε_{mean} (1/a)
Ölgrube - A	50	18.6	4.6	12.2	1.41	1.60	3523	8.2	8.8	0.40	0.033
	75	13.5	5.0	15.7	1.41	1.60	3523	7.6	8.2	0.40	0.025
	100	11.6	5.5	24.7	1.41	1.60	3402	9.5	8.6	0.55	0.022
	125	11.0	4.0	34.9	1.41	1.60	3326	11.6	9.7	0.66	0.019
	150	9.9	3.9	33.2	1.83	1.60	3161	12.6	7.3	0.72	0.022
	175	9.5	5.0	29.2	1.83	1.60	3143	11.1	5.5	0.77	0.026
	200	9.3	5.6	26.5	1.83	1.60	3195	10.2	5.3	1.03	0.039
	225	15.1	5.1	22.5	1.83	1.60	3237	13.8	9.4	1.07	0.048
	250	19.7	5.7	17.0	2.10	1.60	3200	15.8	10.1	1.38	0.081
	275	18.4	6.1	17.3	2.10	1.60	3193	15.3	9.6	1.60	0.092
	300	14.2	6.1	26.2	1.94	1.60	3145	16.0	10.1	1.87	0.071
	325	11.5	6.3	31.4	1.94	1.60	3045	15.4	8.3	1.85	0.059
	350	13.0	5.8	37.3	1.94	1.60	3037	19.9	12.6	2.02	0.054
Kaiserberg - C	300	10.9	8.0	19.0	2.19	1.77	3541	11.5	9.9	0.60	0.032
	325	9.7	7.4	19.7	2.19	1.77	3467	10.4	7.8	0.55	0.028
	350	8.0	5.4	20.7	1.93	1.77	3313	7.5	3.8	0.50	0.024
	375	7.9	5.6	21.4	1.93	1.77	3346	7.7	4.4	0.50	0.023
	400	7.7	8.9	19.9	1.93	1.77	3503	8.0	6.7	0.50	0.025
Reichenkar - A	200	12.2	5.4	26.6	1.90	1.92	3363	14.0	11.0	3.21	0.121
	225	10.7	0.9	30.0	1.90	1.92	3364	11.9	8.9	3.21	0.107
	250	11.9	8.8	24.2	1.83	1.92	3364	13.7	11.0	2.40	0.099
	275	11.7	3.1	26.3	1.83	1.92	3393	11.9	9.5	2.40	0.091
	300	11.0	2.9	25.5	1.83	1.92	3395	10.9	8.5	2.29	0.090
	325	9.8	6.6	25.5	1.62	1.92	3438	10.0	8.9	2.29	0.090
	350	10.4	2.6	25.9	1.77	1.92	3515	10.0	9.4	2.29	0.088
	375	12.1	3.8	22.9	1.77	1.92	3522	10.9	10.3	2.29	0.100

Table 3: Structural and physical parameters along longitudinal profiles of three rock glaciers that were assessed by the same methodology (after Hausmann et. al, 2007) and that were selected to discuss their dynamic behavior. For the list of abbreviations see Appendix A.

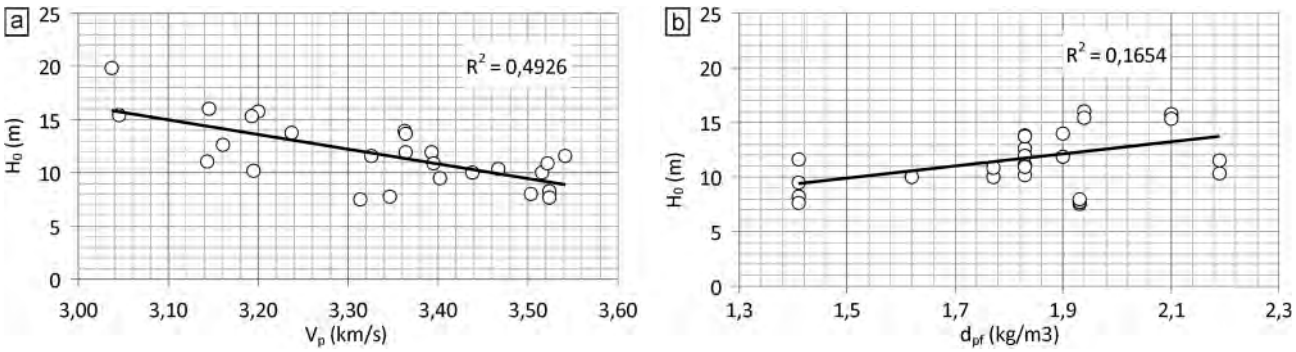

Figure 8: The two best correlations of the assessed physical parameters with the related dynamic parameter H_0 for the two studied rock glaciers and an additional one using the same geophysical methods (Reichenkar rock glacier; Hausmann et al., 2007) as applied in this study. (a) Longitudinal velocity v_p versus H_0 (b) density of the ice-rich permafrost d_{pf} versus H_0.

Table 3:

$$h = dh_{boul} + dh_{pf} \quad (3)$$

$$d = \frac{d_{boul} \cdot dh_{boul} + d_{pf} \cdot dh_{pf}}{h} \quad (4)$$

The quantities dh_{boul} and dh_{pf} in equation (3) describe the thicknesses of the surface debris and the permafrost layer.

The basal shear stress approximated by equation (2) plays an important role in dynamic modelling of glaciers and ice sheets. Frequently, the quantity H_0 (in m)

$$H_0 = \frac{\tau_b}{d_{ice} \cdot g} \quad (5)$$

is used (e.g. Paterson, 1994) to get a rough estimate for the vertical ice thickness by

$$h_{ice} = \frac{H_0}{\cos(\alpha) \cdot \sin(\alpha)} \quad (6)$$

The quantity H_0, as calculated by equations (2 - 5), is included to Table 3 and has a mean value of ~ 12 m. In the next step we analyze correlations between H_0 and the parameter v_p and the density of the permafrost layer (d_{pf}) (Fig. 8). The correlation v_p – H_0 is significant at a 0.1 % level, d_{pf} – H_0 at a 5 % level. The correlation v_p – d_{pf} is not significant, and hence is not shown as cross plot. The existence of the two most significant relations may be interpreted as follows: The three rock glaciers under consideration are active. Higher H_0 means that higher stresses are needed to keep the rock glacier actively creeping. H_0 increases with decreasing P-wave velocity v_p of the permafrost layer (Fig. 8a). A velocity v_p lower than ~ 3500 m/s (temperate ice: 3795 m/s; Kohnen 1974) may be taken as an indicator of an increasing fraction of air in the permafrost layer. Rocky grains and boulders of the permafrost layer come more into contact, internal friction increases, and higher stresses are needed to keep the rock glacier creeping. Thus, to explain the lower P-wave velocities, an increase in air content is more likely than the presence of warmer ice or an increase in water content. In order to keep a degrading rock glacier (reduction of the ice content) in motion a thickening is required.

The correlation d_{pf} – H_0 (Fig. 8b) is not as significant as v_p – H_0. However, increase of H_0 with d_{pf} supports our interpretation of the v_p – H_0 relation. Higher density (> 1500 g/cm³) can be interpreted as lower porosity rock mass with increasing air content but less ice. For permafrost composed of massive ice, the density will consequently trend to a value of 917 g/cm³ (pure glacier ice; Andersland and Ladanyi, 2004), and H_0 will have a minimal value. With respect to the bulk density the lower porosity should over-compensate the loss of ice in the pore space. The least squares regression H_0 versus d_{pf} and v_p is:

$$H_{regression} = 3.1 \cdot d_{pf} - 12.7 \cdot v_p + 48.4 \quad (7)$$

Physical units for d_{pf} and v_p in equation (7) are the same as in Table 3. Before we consider the relation of H_0 with creep velocity v, we reduce H_0 to $H_{0,red}$ for constant v_p = 3500 m/s and d_{pf} = 1500 g/cm³. We further calculate the mean shear deformation within the permafrost layer by

$$\varepsilon_{mean} = \frac{v_{surf}}{h_{pf}} \quad (8)$$

The cross plot of ε_{mean} – $H_{0,red}$ infers a relation between deformation rate and shear stress (Fig. 9). The $H_{0,red}$ – ε_{mean} relation can be approximated by a power law:

$$H_{0,red} = 18.2 \cdot \varepsilon_{mean}^{1/n} \quad (9)$$

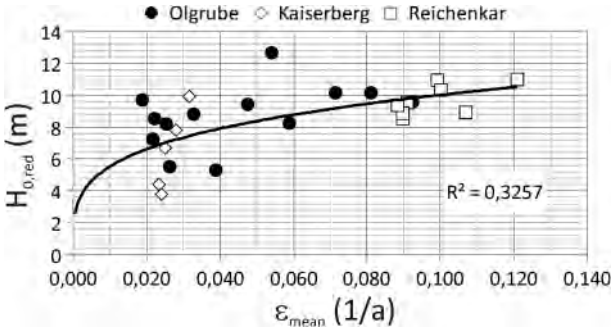

Figure 9: Relation between values for the shear stress ($H_{0,red}$) and the deformation rate ($å_{mean}$) for the rock glaciers Ölgrube, Kaiserberg and Reichenkar. The approximated power law corresponds to a creep exponent of n=3.9.

The reciprocal exponent is n=3.9 and is near to exponents for Glen's law for pure ice (n=3; Hooke, 1981; Budd and Jacka, 1989) and within the range of exponents from permafrost cores in Alpine rock glaciers ($1.9 < n < 4.5$; Arenson and Springman, 2005b). The power law fits the data very well, is significant at a 0.1 % level, and the remaining residuals do no longer show any systematic trend. With equation (9) we can predict the creep velocity within a range of ± 25 %. This is notable, as errors from the geophysical model also exist. As we use a simple approach where shear stress increases with depth and where the shear stress at the permafrost base is a parameter for the deformation, possible shear horizons are not considered in the permafrost layer.

In a next step we analyze and discuss the GPR-reflection of the permafrost layer and its relation with the physical parameters v_p and d_{pf}, which are related to ductility and ice content of this layer (Fig. 10). The observed GPR-reflections can be divided into the following types: (i) reflectors parallel to the surface, (ii) upward dipping or concave reflectors, (iii) downward dipping reflectors, and (iv) undulating and chaotic reflections. The origin of internal reflectors in rock glaciers has been interpreted as debris inclusions along thrust planes (Maurer and Hauck, 2007; Fukui et al., 2008; Monnier et al., 2008, 2011; Krainer et al., 2010). Isaksen et al. (2000) explain the formation of layers oriented parallel or slanting downwards in relation to the rock glacier surface by accumulation of seasonal snow that was buried and compacted by falling rocks and boulders. At Ölgrube rock glacier long reflectors parallel to the surface (i) are found in regions with high P-wave velocity and low density, indicating zones with high ice content. Typical P-wave velocity values for ice-rich zones in rock glaciers are 3700 m/s (Vonder Mühll and Holub, 1992) and 3795 m/s for temperate glaciers (Kohnen, 1974). In general, the recent flow velocities do not correlate with the length of the surface-parallel reflectors. For the Kaiserberg rock glacier this type of GPR-reflection is found in the rooting zone and where the P-wave velocity is high. In the upper and lower part of the Ölgrube rock glacier, concave reflectors (ii) are found at the end of long subsurface-parallel reflectors (at 150 and 350 m). However, the occurrence of shallow shear zones can be excluded due to the insufficient shear stress at this depth. Concave reflectors are interpreted as an expression of strong compres-

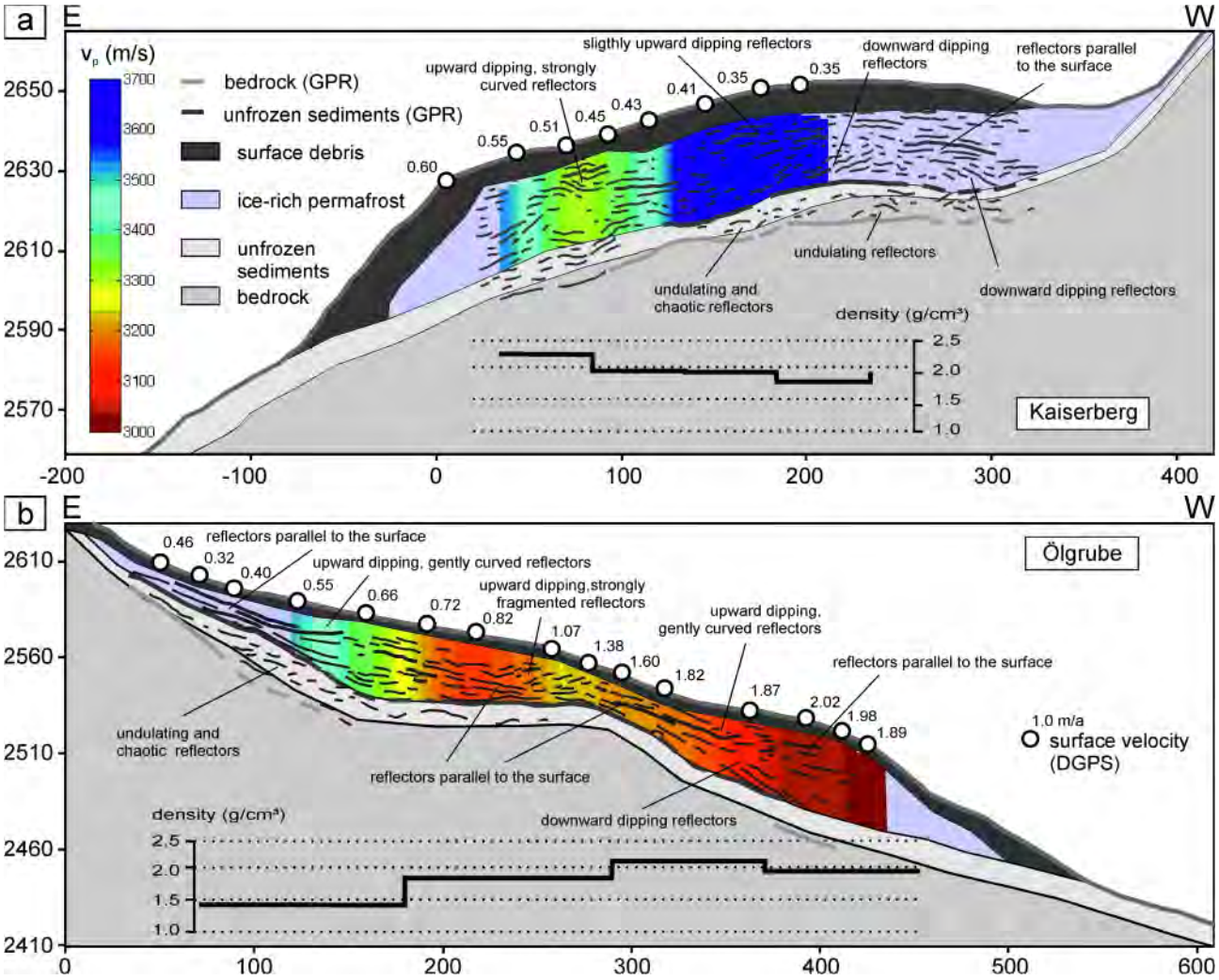

Figure 10: Compilation of the GPR-reflection of the permafrost layer with the physical parameters v_p (longitudinal velocity) and d_{pf} (permafrost density) for the rock glaciers Kaiserberg (a) and Ölgrube (b).

sion (Monnier et al., 2011). For Ölgrube rock glacier the surface velocity clearly exhibits an extensional flow field. Thus, these structures may originate from alignment of debris and do not represent the actual stress field. For Kaiserberg the upward dipping curved reflector (at 95 m) is located close to a ridge. Nearby measurements of the surface velocity indicate an extensional flow field at the frontal part. As shown above, the thickness of the rock glacier at the frontal part of Ölgrube has to increase to keep the rock glacier creeping. This view is supported by the clearly imaged downward (iii) and surface-parallel directed reflectors and a surface topography whose angle is flatter than the bedrock surface. However, at both rock glaciers the bedrock surface steepens at the front and this may also contribute to the increase of the flow velocity. However, this would not explain the thickening. Further, Figure 6a shows that although the bedrock surface is imaged uniformly, large variations in surface velocities were observed. This seems to be caused rather by the thickness and density of the ice-rich permafrost than by the bedrock surface. At the Kaiserberg rock glacier this signature is found in the frontal part and in the rooting zone of the rock glacier where a depression is developed.

At both rock glaciers the GPR-reflection (recorded in winter) clearly separates the ductile ice-rich permafrost (surface-parallel reflectors, concave reflectors) from the ice-free sediments underneath (undulating and chaotic reflections, iv). Further, their reflectivity is uniform along the longitudinal profiles, but the length and direction of the GPR-reflection is different. From Figures 8 and 9 we interpret that air content, ice content, and porosity of the rock mass might change along the profiles, but that water is uniformly distributed. This would explain why the reflectivity (depends on material properties) is uniform and the GPR-reflection (representing the structure) changes along the longitudinal profiles.

In Hausmann et al. (2007) a first assessment of uncertainties of the applied geophysical model was given. This includes random errors of the associated geophysical parameters and their effect on the estimated ice content. Excluding the ice content, the computed values for the Reichenkar rock glacier are also representative for this study. The standard deviation for the volumetric ice contents are ±10 % for Ölgrube rock glacier and ±18 % for Kaiserberg rock glacier. We show that systematic errors of the structural and physical parameters do not play a dominant role in this study. This is indicated by the high correlation coefficient (R=0.7) between the structural / physical parameters and the dynamic ones (Figs 8a, 9). Note that these cross plots use parameters that were obtained independently from three active rock glaciers and that their creep behaviour can be explained and described together using equations (7, 9) within a range of ± 25 %. Further, a reliable creep exponent was found for these rock glaciers. In chapter 5 we used a constant density for the surface debris and the ice-free sediments. As both layers are small compared to the ice-rich permafrost, the impact of density variations in these layers is small. For example, a change of 20 % in the density of the surface debris layer would result in only 4 % of the density of the ice-rich permafrost layer. In section 3.1 we state that the basal GPR reflector can be used to confirm the presence of the 4 layers. Since the derived 1D velocity models focus on the depth to the ice-free sediment layer, the depth to the underlying basal reflector is probably shallower. For example, a 10 m thick layer of fine-grained, ice-free deposits with an interval velocity of 0.09 m/ns (Hauck and Kneisel, 2008) changes the thickness only by about 4 m.

7. Conclusions

The geophysical concept introduced by Hausmann et al. (2007) was applied successfully to establish 4-layer models for the two investigated rock glaciers Ölgrube and Kaiserberg. For both rock glaciers an ice-free sediment layer had to be introduced below the ice-rich permafrost body. A confirmation of the 4 layers was found in areas where the bedrock surface was resolved by GPR and seismic refraction. The geophysical models provided relevant information on structural and physical parameters and helped to understand dynamic processes of the rock glacier.

For both rock glaciers we found 4 layers to be composed of 4 - 6 m surface debris (“active layer”), 20 - 30 m ice-rich permafrost, and 10 - 15 m ice-free sediments. The average depth to the bedrock surface is 35 - 50 m. The geophysical model of the Ölgrube rock glacier exhibits large changes in thickness of the ice-rich permafrost, density and P-wave velocity of the permafrost in flow direction. Along the cross section, the thickness of the ice-rich permafrost increases and the density of the ice-rich permafrost decreases from NE to SW. We estimated a volumetric ice content of 43 % in the frontal part and 61 % in the root zone. For the Kaiserberg rock glacier the geophysical model detected only slight structural changes of the thickness of the ice-rich permafrost along both profiles. The density of the ice-rich permafrost decreases towards N in the cross section and increases from N to E in flow direction. The ice content varies laterally between about 40 and 50 %.

The recent flow fields clearly show an extensional flow field for both rock glaciers near their frontal parts. The geophysical model combined with the flow field further provides details on the movement of the rock glacier: The steeper surface slope at profile A of Ölgrube rock glacier (310 m) is caused by a rise in the bedrock topography and results in a thinning of the thickness of the ice-rich permafrost. At the Kaiserberg rock glacier the formation of major lobes indicates creep of the rock glacier from S to N in former times. The assessed internal structures explain why the recent flow field is directed exclusively towards E (along profile C).

In this study, structural and physical parameters assessed by surface based geophysical methods are used to explain the dynamics of the rock glacier. From the two studied active rock glaciers and an additional rock glacier (Reichenkar rock glacier; located 25 km to the NE of Ölgrube rock glacier), which was investigated by applying the same methodology (Hausmann et al., 2007), we found that a quantity related to the

shear stress at the permafrost base describes their creep behaviour. Correlations of this quantity with the P-wave velocity and the density of the ice-rich permafrost have shown that the three geophysical models are conclusive. Regarding the creep behaviour of these active rock glaciers, a reduction of ice involves increased internal friction, lower P-wave velocities, and higher bulk densities. In this case a thickening is required in order to keep the rock glacier in motion. The relation between deformation rate and shear stress is approximated by a power law and results in a creep exponent of 3.9.

The GPR-reflection pattern of the permafrost layer can be summarized as follows: Long reflectors parallel to the surface are found in regions with high P-wave velocity and low density, indicating zones with high ice content. The source of the shallow concave reflectors is unclear, but they do not correspond to the actual stress field. The effect of thickening near the front part of Ölgrube can be clearly imaged by reflectors directed parallel and downwards to the surface. At both studied rock glaciers the GPR-reflections separate the ductile ice-rich permafrost from the ice-free sediments underneath.

Acknowledgements

The investigations were funded by the 'Fonds zur Förderung der wissenschaftlichen Forschung' FWF (Austrian Science Foundation), project P 15218 and the Österreichische Akademie der Wissenschaften (Austrian Academy of Science), ISDR project 'Permafrost in Austria'. The authors wish to express their special thanks to M. Behm and W. Chwatal who were helpful during the processing and P. Mendes-Cerveira and W. Mostler for field assistance. We further thank R. Meurers and B. Meurers for their comments and F. Thalheim for editing the English text. We acknowledge the comments of the two anonymous reviewers that helped to improve the manuscript significantly.

References

Andersland, O.B. and Ladanyi, B., 2004. Frozen Ground Engineering. John Wiley & Sons, Inc., Second edition, 363 pp.

Archie, G.E., 1942. The electrical resistivity log as an aid in determining some reservoir characteristics. Petroleum Transactions of AIME, 146, 54-62.

Arenson, L. and Jakob, M., 2010. The significance of rock glaciers in the dry Andes – A discussion of Azocar and Brenning (2010). Permafrost and Periglacial Processes, 21, 286-288, doi:10.1002/ppp.69.

Arenson, L., Hoelzle, M. and Springman, S., 2002. Borehole deformation measurements and internal structure of some rock glaciers in Switzerland. Permafrost and Periglacial Processes, 13, 117-135, doi: 10.1002/ppp.414.

Arenson, L. and Springman, S., 2005a. Triaxial constant stress and constant strain rate tests on ice-rich permafrost samples. Canadian Geotechnical Journal, 42, 412-430.

Arenson, L. and Springman, S., 2005b. Mathematical descriptions for the behaviour of ice-rich frozen soils at temperatures close to 0 °C. Canadian Geotechnical Journal, 42, 431-442.

Azocar, G.F. and Brenning, A., 2010. Hydrological and geomorphological significance of rock glaciers in the dry Andes, Chile (27°–33°S). Permafrost and Periglacial Processes, 21, 42-53, doi:10.1002/ppp.66.

Barsch, D., Fierz, H. and Haeberli, W., 1979. Shallow core drilling and bore-hole measurements in the permafrost of an active rock glacier near the Grubengletscher, Wallis, Swiss Alps. Arctic and Alpine Research, 11, 215-228.

Barsch, D., 1996. Rockglaciers. Indicators for the Present and Former Geoecology in High Mountain Environments. Springer-Verlag, Berlin, 331 pp.

Barsch, D. and Jakob, M., 1998. Mass transport by active rockglaciers in the Khumbu Himalaya. Geomorphology, 26, 215-222.

Berger, J., 2002. Aufbau und Dynamik aktiver Blockgletscher am Beispiel der Blockgletscher in der Inneren Ölgrube und dem Kaiserbergtal (Ötztaler Alpen/Tirol). Unveröff. Diplomarbeit, Institut für Geologische Wissenschaften der Ernst-Moritz-Arndt-Universität Greifswald, 129 S.

Berger, J., Krainer, K. and Mostler, W., 2004. Dynamics of an active rock glacier (Ötztal Alps, Austria). Quaternary Research, 62, 233-242.

Berthling, I., Etzelmüller, B., Isaksen, K. and Sollid, J.L., 2000. Rock glaciers on Prins Karls Forland. II: GPR Soundings and the Development of Internal Structures. Permafrost and Periglacial Processes, 11, 357-369. doi: 10.1002/1099-1530(200012).

Berthling, I., Etzelmüller, B., Wale, M. and Sollid, J.L., 2003. Use of ground penetrating radar (GPR) soundings for investigating internal structures in rock glaciers. Examples from Prins Karls Forland, Svalbard. Zeitschrift für Geomorphologie, 132, 103-121.

Brenning, A., 2005. Geomorphological, hydrological and climatic significance of rock glaciers in the Andes of central Chile (33-35°S). Permafrost and Periglacial Processes, 16, 231-240. doi: 10.1002/ppp.528.

Budd W. F. and Jacka T. H., 1989. A review of ice rheology for ice sheet modelling. Cold Regions Science and Technology, 16, 107–144.

Burger, K.C., Degenhard,t J.J. and Giardino, J.R., 1999. Engineering geomorphology of rock glaciers. Geomorphology, 31, 93-132.

Croce, F.A. and Milana, J.P. 2002. Internal structure and behaviour of a rock glacier in the Arid Andes of Argentina. Permafrost and Periglacial Processes, 13, 289-299.

Degenhardt, J.J. and Giardino, J.R., 2003. Subsurface investigation of a rock glacier using ground-penetrating radar: Implications for locating stored water on Mars. Journal of Geophysical Research, 108, 8038-8055, doi:10.1029/2002JE001888.

Degenhardt, J.J., Giardino J.R., Berthling, I., Isaksen, K., Ødegard, R.S. and Sollid, J.L., 2002. The internal structure of rock glaciers and geomorphologic interpretations: Yankee Boy Basin, CO, USA and Hiorthfjellet and Prins Karls Forland, Svalbard. The Geological Society of America (GSA), 34.

Evin, M., Fabre, D. and Johnson, P.G., 1997. Electrical resistivity measurements on the rock glaciers of Grizzly Creek, St Elias Mountains, Yukon. Permafrost and Periglacial Processes, 8, 179-189.

Farbrot, H., Isaksen, K., Eiken, T., Kääb, A. and Sollid, J. L., 2005. Composition and internal structures of a rock glacier on the strandflat of western Spitsbergen, Svalbard. Norwegian Journal of Geography (Norsk Geografisk Tidsskrift), 59, 139-148.

Finsterwalder, S., 1928. Begleitworte zur Karte des Gepatschferners. Zeitschrift für Gletscherkunde, 16, 20-41.

Francou, B., Fabre, D., Pouyaud, B., Jomelli, V. and Arnaud, Y., 1999. Symptoms of degradation in a tropical rock glacier, Bolivian Andes. Permafrost and Periglacial Processes, 10, 91-100.

Fukui, K., Sone, T., Strelin, J-A., Torielli, C-A., Mori, J. and Fujii, Y., 2008. Dynamics and GPR stratigraphy of a polar rock glacier on James Ross Island, Antarctic Peninsula. Journal of Glaciology, 54, 445-451.

Götze, H.-J. and Lahmeyer, B., 1988. Application of three-dimensional interactive modeling in gravity and magnetics. Geophysics, 53, 1096-1108.

Granser, H., Meurers, B. and Steinhauser, P., 1989. Apparent density mapping and 3d gravity inversion in the Eastern Alps. Geophysical Prospecting, 37, 279-292.

Haeberli, W., Hallet, B., Arenson, L., Elconin, R., Humlum, O., Kääb, A., Kaufmann, V., Ladanyi, B., Matsuoka, N., Springman, S., and Vonder Mühll, D., 2006. Permafrost creep and rock glacier dynamics. Permafrost and Periglacial Processes, 17, 189-214, doi: 10.1002/ppp.561.

Haeberli, W., 1990. Glacier and permafrost signals of the 20th-century warming. Annals of Glaciology, 14, 99-101.

Haeberli, W., Huder, J., Keusen, H.R., Pika, J. and Röthlisberger, H., 1988. Core drilling through rock glacier permafrost. In: 5th International Conference on Permafrost, Proceedings 2, Trondheim, Norway, Tapir Publishers, 937-942.

Haeberli, W., Guodong, C., Gorbunov, A.P. and Harris, S.A., 1993. Mountain permafrost and climatic change. Permafrost and Periglacial Processes, 4, 165-174.

Hauck, C., and Kneisel, C., 2008. Applied Geophysics in Periglacial Environments. Cambridge University Press, New York, 256 pp.

Hauck, C. and Vonder Mühll, D. 1999. Detecting Alpine permafrost using electromagnetic methods. In: Advances in cold regions thermal engineering and sciences, (eds. K. Hutter, Y. Wang, H. Beer), 475-482, Springer Verlag, Heidelberg.

Hauck, C. and Vonder Mühll, D., 2003a. Evaluation of geophysical techniques for application in mountain permafrost studies. Zeitschrift für Geomorphologie, Suppl.-Bd., 132, 161-190.

Hauck, C. and Vonder Mühll, D., 2003b. Inversion and interpretation of two-dimensional geoelectrical measurements for detecting permafrost in mountainous regions. Permafrost and Periglacial Processes, 14, 305-318. doi: 10.1002/ppp.462.

Hauck, C., Vonder Mühll, D. and Maurer, H., 2003. DC resistivity tomography to detect and characterize mountain permafrost. Geophysical Prospecting, 51, 273-284.

Hauck, C, Isaksen, K, Vonder Mühll, D., Sollid, J.L., 2004. Geophysical surveys designed to delineate the altitudinal limit of mountain permafrost: an example from Jotunheimen, Norway. Permafrost and Periglacial Processes, 15, 191-205. doi: 10.1002/ppp.493.

Hauck, C., Böttcher, M. and Maurer, H., 2011. A new model for estimating subsurface ice content based on combined electrical and seismic data sets. The Cryosphere, 5, 453-468, doi:10.5194/tc-5-453-2011.

Hausmann, H., Krainer, K., Brückl, E. and Mostler, W., 2007. Internal structure and ice content of Reichenkar Rock Glacier (Stubai Alps, Austria) assessed by geophysical investigations. Permafrost and Periglacial Processes, 18, 351-367, doi: 10.1002/ppp.60.

Hilbich, C., 2010. Time-lapse refraction seismic tomography for the detection of ground ice degradation. The Cryosphere, 4, 243-259.

Hilbich, C., Hauck, C., Scherler, M., Schudel, L., Völksch, I., Hoelzle, M., Vonder Mühll, D, and Mäusbacher, R., 2008. Monitoring mountain permafrost evolution using electrical resistivity tomography: A seven-year study of seasonal, annual and long-term variations at Schilthorn, Swiss Alps. Journal of Geophysical Research, 113, F01S90, doi:10.1029/2007JF00079.

Hilbich, C., Marescot, L., Hauck, C., Loke, M.H. and Mäusbacher, R., 2009. Applicability of electrical resistivity tomography monitoring to coarse blocky and ice-rich permafrost landforms. Permafrost and Periglacial Processes, 20(3), 269-284, doi: 10.1002/ppp.652.

Hooke, R.L.B., 1981. Flow law for polycrystalline ice in glaciers: comparison of theoretical predictions, laboratory data, and field measurements. Reviews of Geophysics and Space Physics, 19, 664-672.

Hoinkes, G. and Thöni, M., 1993. Evolution of the Ötztal-Stubai, Scarl-Campo and Ulten Basement Units. In: Pre-Mesozoic Geology in the Alps, Raumer, J.F. and Neubauer, F. (eds.), Springer, Berlin, 485-494.

Ikeda, A., 2006. Combination of conventional geophysical methods for sounding the composition of rock glaciers in the Swiss Alps. Permafrost and Periglacial Processes, 17, 35-48, doi: 10.1002/ppp.550.

Isaksen, K., Ødegard, R.S., Eiken, T., and Sollid, J.L., 2000. Composition, flow and development of two tongue-shaped rock glaciers in the permafrost of Svalbard. Permafrost and Periglacial Processes, 11, 241-257.

Kirchheimer, F., 1988a. 3-D refraction statics by weighted least-squares inversion. SEG Expanded Abstracts, 7, 794.

Kirchheimer, F., 1988b. A tomographic approach to 3-D refraction statics. 5th Annual Meeting of the European Association of Exploration Geophysicists, Proceedings, The Hague, Netherlands.

Klingele, E. and Vonder Mühll, D., 1993. Gravimetrische Untersuchungen im Permafrost des Blockgletschers Murtèl-Corvatsch (Oberengadin). Vermessung, Photogrammetrie, Kulturtechnik, 91, 575-580.

Kneisel, C., Hauck, C., Fortier, R. and Moorman, B.J., 2008. Advances in geophysical methods for permafrost investigations. Permafrost and Periglacial Processes, 19, 157-178, doi: 10.1002/ppp.61.

Kohnen, H., 1974. The temperature dependence of seismic waves in ice. Journal of Glaciology, 13, 144–147.

Krainer, K. and Mostler, W., 2000. Reichenkar rock glacier: a glacier derived debris-ice system in the Western Stubai Alps, Austria. Permafrost and Periglacial Processes, 11, 267-275.

Krainer, K. and Mostler, W., 2002. Hydrology of active rock glaciers: Examples from the Austrian Alps. Arctic, Antarctic, and Alpine Research, 34, 142-149.

Krainer, K. and Mostler, W., 2006. Flow velocities of active rock glaciers in the Austrian Alps. Geografiska Annaler, 88 A, 267–280, doi: 10.1111/j.0435-3676.2006.00300.x.

Krainer, K., Mostler, W. and Span, N., 2002. Dynamik und Entstehung aktiver Blockgletscher – ein Beispiel aus dem Inneren Reichenkar (westliche Stubaier Alpen, Tirol). – 44. Tagung der Hugo Obermaier-Gesellschaft, Innsbruck, 2.-6.4.2002, Abstract zur Posterpräsentation.

Krainer, K., Mostler, W. and Spötl, C., 2007. Discharge from active rock glaciers, Austrian Alps: A stable isotope approach. Austrian Journal of Earth Sciences, 100, 102-112.

Krainer, K., Lang, K. and Hausmann, H., 2010. Active rock glaciers at Croda Rossa/Hohe Gaisl, Eastern Dolomites (Alto Adige/South Tyrol, Northern Italy). Geografia Fisica e Dinamica Quaternaria, 33, 25-36.

Lehmann, F. and Green, A.G., 2000. Topographic migration of georadar data: Implications for acquisition and processing. Geophysics, 65, 836-848.

Leopold, M., Williams, W., Caine, N., Völkel, J. and Dethier, D., 2011. Internal structure of the Green Lake 5 rock glacier, Colorado Front Range, USA. Permafrost and Periglacial Processes, 22, 107-119, doi: 10.1002/ppp.706.

Maurer, H. and Hauck, C., 2007. Geophysical imaging of alpine rock glaciers. Journal of Glaciology, 53, 110-120.

Monnier, S., Camerlynck, C. and Rejiba, F., 2008. Ground penetrating radar survey and stratigraphic interpretation of the Plan du Lac Rock Glaciers, Vanoise Massif, Northern French Alps. Permafrost and Periglacial Processes, 19, 19-30, doi: 10.1002/ppp.61.

Monnier, S., Camerlynck, C., Rejiba, F., Kinnard, C., Feuillet, T. and Dhemaied, A., 2011. Structure and genesis of the Thabor rock glacier (Northern French Alps) determined from morphological and ground-penetrating radar surveys. Geomorphology, 134, 3-4, 269-279, doi:10.1016/j.geomorph.2011.07.004.

Musil, M., Maurer, H., Green, A.G. , Horstmeyer, H., Nitsche, F.O., Vonder Mühll, D. and Springman, S., 2002. Shallow seismic surveying of an Alpine rock glacier. Geophysics, 67, 1701-1710.

Musil, M., Maurer, H., Hollinger, K. and Green, A.G., 2006. Internal structure of an alpine rock glacier based on crosshole georadar traveltimes and amplitudes. Geophysical Prospecting, 54, 273-285.

Otto, J.-C., Schrott, L., Jaboyedoff, M. and Dikau, R., 2009. Quantifying sediment storage in a high alpine valley (Turtmanntal, Switzerland). Earth Surface Processes and Landforms, 34, 1726-1742, doi: 10.1002/esp.185.

Otto, J.-C. and Sass, O., 2006. Comparing geophysical methods for talus slope investigations in the Turtmann valley (Swiss Alps). Geomorphology, 76, 257-272. doi: 10.1016/j.geomorph.2005.11.

Paterson, W.S.B., 1994. The Physics of Glacier (3nd Edition). Butterworth Heinemann, Elsevier Science, United States of America. 496 pp.

Pillewizer, W., 1957. Untersuchungen an Blockströmen der Ötztaler Alpen. Geomorphologische Abhandlungen des Geographischen Institutes der FU Berlin (Otto-Maull-Festschrift) 5, 37-50.

Potter, N., 1972. Ice-Cored Rock Glacier, Galena Creek, Northern Absaroka Mountains, Wyoming. Geological Society of America Bulletin, 83, 3025-3058.

Ribolini, A., Chelli, A., Guglielmin, M. and Pappalardo, M., 2007. Relationships between glacier and rock glacier in the Maritime Alps, Schiantala Valley, Italy. Quaternary Research, 68, 353-363, doi: 10.1016/j.yqres.2007.08.004.

Röthlisberger, H., 1972. Seismic exploration in cold regions. Cold Regions Science and Monographs, II-A2a, Hannover, 139 pp.

Scapozza, C., Lambiel, C., Baron, L., Marescot, L. and Reynard, E., 2011. Internal structure and permafrost distribution in two alpine periglacial talus slopes, Valais, Swiss Alps. Geomorphology, 132), 208-221, doi: doi:10.1016/j.geomorph.2011.05.010.

Telford, W.M., Geldard, L.P. and Sheriff, R.E., 1990. Applied Geophysics. Cambridge University Press, New York, 792 pp.

Timur, A., 1968. Velocity of compressional waves in porous media at permafrost temperatures. Geophysics, 33, 584-595.

Tonidandel, D., Leiter, J., Mair, V. and Lang, K., 2010. Erste Ergebnisse der Kernbohrungen auf dem aktiven Blockgletscher in Lazaun, Schnalstal (Südtirol). Geo. Alp 7, 106-107.

Vonder Mühll, D., 1996. Drilling in alpine permafrost. Norwegian Journal of Geography (Norsk Geografisk Tidsskrift), 50, 17-24. doi:10.1080/0029195960855234.

Vonder Mühll, D., Hauck, C. and Gubler, H., 2002. Mapping of mountain permafrost using geophysical methods. Progress in Physical Geography, 26, 643-660, doi: 10.1191/0309133302 pp356ra.

Vonder Mühll, D., Hauck, C., Gubler, H., McDonald, R. and Russill, N., 2001. New geophysical methods of investigating the nature and distribution of mountain permafrost with special reference to radiometry techniques. Permafrost and Periglacial Processes, 12, 27-38, doi:10.1002/ppp.38.

Vonder Mühll, D., Hauck, C. and Lehmann, F., 2000. Verification of geophysical models in Alpine permafrost using borehole information. Annals of Glaciology, 31, 300-306.

Vonder Mühll, D. and Holub, P., 1992. Borehole logging in Alpine permafrost, Upper Engadin, Swiss Alps. Permafrost and Periglacial Processes, 3, 125-132.

Watkins, J.S., Walters, L.A. and Godson, R.H., 1972. Dependency of in-situ compressional-wave velocity on porosity in unsaturated rocks. Geophysics, 37, 29-35.

Yilmaz, Ö., 2001. Seismic data analysis, 2nd edition. Society of Exploration Geophysicists, United States of America, 2027 pp.

Received: 19 December 2011
Accepted: 7 September 2012

Helmut HAUSMANN[1)4)*)], Karl KRAINER[2)], Ewald BRÜCKL[1)] & Christian ULLRICH[3)]

[1)] Institute of Geodesy and Geophysics, Vienna University of Technology, Vienna, Austria;

[2)] Institute of Geology and Paleontology, University of Innsbruck, Innsbruck, Austria;

[3)] Federal Office of Metrology and Surveying (BEV), Vienna, Austria;

[4)] Central Institute for Meteorology and Geodynamics (ZAMG), Vienna, Austria;

[*)] Corresponding author, helmut.hausmann@zamg.ac.at

Appendix

Appendix A: List of symbols

α	surface slope
d_{boul}	density of the surface debris layer
d_{pf}	density of the ice-rich permafrost
d_{ice}	density of the pure ice
dh_{boul}	thickness of the surface debris layer
dh_{pf}	thickness of the ice-rich permafrost
ε_{mean}	mean strain deformation
Φ	fractional porosity
h_{bed}	depth to the bedrock surface
H_0	quantity related to the shear stress at the permafrost base and a density of pure ice
$H_{0,red}$	H_0 reduced to constant v_P and d_{pf}
i	relative ice content of the ice-rich permafrost
v_{GPR}	electromagnetic wave speed of the ice-rich permafrost
v_P	seismic P-wave velocity of the ice-rich permafrost
v_{surf}	surface velocity observed by DGPS
X	profile offset